Sniffing is initiated by the actions of dopamine on ventral striatum neurons

Authors: Natalie L. Johnson[1], Anamaria Cotelo-Larrea[1], Lucas A. Stetzik[1], Umit M. Akkaya[2], Adrienn G. Varga[3], Minghong Ma[4], and Daniel W. Wesson[1,*]

Affiliations:

[1]Department of Pharmacology and Therapeutics, Center for Smell and Taste, Center for Addiction Research and Education; University of Florida College of Medicine, Gainesville, FL 32610, USA

[2]Department of Computer Engineering, Gebze Technical University, 41400 Kocaeli, Turkey

[3]Department of Neuroscience, Breathing Research and Therapeutics Center; University of Florida College of Medicine, Gainesville, FL 32610, USA

[4]Department of Neuroscience, Perelman School of Medicine, University of Pennsylvania, Philadelphia, PA 19104, USA

[*]Corresponding author: Email: danielwesson@ufl.edu

Abstract:
Sniffing is a motivated behavior displayed by all terrestrial vertebrates on the planet. While sniffing is associated with acquiring and processing odors, sniffing is also intertwined with affective and motivated states. The neuromodulatory systems which influence the display of sniffing are unclear. Here, we report that dopamine release into the ventral striatum, with exception of the nucleus accumbens core, is coupled with bouts of sniffing and that stimulation of dopaminergic terminals in those regions initiates sniffing. The activity of post-synaptic D1 and D2 receptor-expressing neurons in the ventral striatum is also coupled with sniffing and antagonism of ventral striatum D1 and D2 receptors squelches sniffing behavior. Together, these results support a model whereby sniffing is initiated by dopamine's actions upon ventral striatum neurons. The nature of sniffing being integral to both olfaction and motivated behaviors implicates this circuit in a wide array of functions.

One-Sentence Summary: Mesolimbic dopamine input to the ventral striatum supports the highly conserved behavior of sniffing by promoting both the initiation and vigor of sniffing bouts.

Introduction

Sniffing is a volitional behavior displayed by all terrestrial vertebrates and is defined by the rapid inhalation and exhalation of air through the nose. The commonplace function ascribed to sniffing is that it aids in perceiving odors (Uchida et al., 2006; Wachowiak, 2011). This is supported by studies reporting that rodents increase their respiratory frequency from ~2-4Hz at rest, up into an around 6-12Hz range when sampling an odor (Welker, 1964; Youngentob et al., 1987; Kepecs et al., 2007; Wesson et al., 2008). In addition to supporting olfaction, sniffing is also intertwined with affective and motivated states wherein sniffing is considered an appetitive behavior (Clarke and Trowill, 1971; Ikemoto and Panksepp, 1994; Isles et al., 2001). For instance, rodents, dogs, and even semi-aquatic vertebrates increase their sniffing frequency while foraging for food and in anticipation of reinforcers in instrumental tasks (Ikemoto and Panksepp, 1994; Catania, 2006; Kepecs et al., 2007; Wesson et al., 2008). The frequency of sniffing also appears to influence emotional states (Moberly et al., 2018; Ashhad et al., 2022). Furthermore, sniffing serves as a "master clock" for essential physiological rhythms including whisking, wherein the rhythm of sniffing is coupled with whisking and also other head movements (Moore et al., 2013; Kleinfeld et al., 2016). Therefore, it is clear that sniffing holds a ubiquitous position in nature.

The coordination of respiration, and the tight control of the inspiratory / post-inspiratory / expiratory rhythm, are afforded by brainstem structures which elegantly time breaths, control their depth, and send these instructive signals toward the breathing plant by means of the spinal and cranial nerve (Del Negro et al., 2018; Ramirez and Baertsch, 2018). Those respiratory brainstem structures are critical for the orchestration of sniffing. A major quest for understanding the neural basis for sniffing remains, and that is to determine the modulatory circuitry which invigorates an animal to go from basal breathing that serves the purpose of gas exchange to engage in the voluntary act of sniffing.

We reasoned the mesolimbic dopamine (DA) system as a prime candidate for the invigoration of sniffing. Neurons synthesizing DA in the ventral tegmental area (VTA) project into the basal forebrain, including into the ventral striatum. The ventral striatum, considered a limbic-motor interface (Mogenson et al., 1980), is well-known to integrate cortical and limbic circuitry to adaptively guide behavior (Ikemoto, 2007; Haber, 2011). The major subcomponents of the ventral striatum, including the nucleus accumbens (NAc) and the tubular striatum (TuS; also known as the olfactory tubercle) are recipient of dense DAergic inputs from the VTA. Neurons in both the NAc and TuS are largely spiny projection neurons expressing D1- or D2-like receptors which mediate actions of DA (Zahm and Heimer, 1987; Mingote et al., 2015; Wieland et al., 2015). Through studies of DA's role in the ventral striatum, we have come to learn that DA's actions in the ventral striatum influence reinforcement, motivation, aversion behaviors, and also cellular plasticity needed for learning (Phillips et al., 2003; Wise, 2004; Stuber et al., 2010; Lobo and Nestler, 2011; Menegas et al., 2017; Morales and Margolis, 2017). DAergic manipulations in the ventral striatum also influence exploratory behaviors in open-field and other gross motor behavior assays and recently it was reported that DAergic inputs regulate whisking (Li et al., 2023). Mesolimbic DA thus seems a quintessential neural system for supporting sniffing. Here, we investigated the role of mesolimbic DA in the display of sniffing behavior to find that sniffing is initiated by DA's actions upon ventral striatum neurons.

Results

Sniffing vigor is associated with mesolimbic DA release

We initially sought to understand the relationship between sniffing and DA release in the ventral striatum. To address this, we first performed a tracing study to identify ventral striatum subregions wherein DA inputs terminate for subsequent monitoring of DA during behavior. It is well known especially in rats that the ventral striatum receives dense input from mesolimbic DAergic neurons (Ikemoto, 2007; Watabe-Uchida et al., 2012) and that DA dynamics may differ between ventral striatum subregions (Lammel et al., 2011; Badrinarayan et al., 2012). To address this, we injected AAV1-hSyn-FLEX-mGFP-2A-Synaptophysin-mRuby into the VTA of DAT^{IRES}-Cre mice (**Fig 1A & Fig S1**). This approach allowed for visualization of fluorescent puncta, which indicate DAergic presynaptic terminals, throughout the TuS and NAc (**Fig 1B**). The injections resulted in GFP expression throughout the VTA (**Fig S1**). We quantified fluorescent puncta in the NAc Core (NAcC), NAc Shell (NAcSh), medial TuS (mTuS), and lateral TuS given different roles for these subregions in the regulation of motivated behaviors (**Fig 1C**) (Ikemoto, 2003; Floresco, 2015; Murata et al., 2015; Wesson, 2020). We observed robust fluorescence, indicating synaptophysin+ DAT VTA terminals, in the TuS and NAc, most notably in the anterior aspect of the mTuS and NAc (**Fig 1C**) with 113% and 78% more innervation in the anterior versus posterior halves of the mTuS and NAcSh, respectively (the anterior or posterior-most 200µm were used for quantification of these regions). Following this we focused analyses on the anterior aspect of both structures. While the mTuS was rich with synaptophysin+ DAT VTA terminals, this contrasted to the lateral TuS which was largely void of innervation (**Fig 1C & 1D**, rmANOVA $F(1.52, 7.6)=31.74$ $p=0.0003$, Tukey's multiple comparisons ant mTuS vs. ant LatTuS $p=0.014$). Comparable amounts of synaptophysin+ DAT VTA terminals were found in the anterior NAcSh and anterior NAcC (**Fig 1C & 1D**, Tukey's multiple comparisons antNAcSh vs. antNAcC, $p=0.073$). The density of input across the anteromedial aspects of the TuS, NAcSh, and NAcC were all similar (**Fig 1C & 1D;** Tukey's multiple comparisons anterior mTuS vs. anterior NAcSh $p=0.217$; anterior mTuS vs. anterior NAcC $p=0.878$). Together the anterior NAcSh, NAcC, and mTuS are the major recipients of VTA DAergic input in the ventral striatum.

Having established this, we next sought to investigate the temporal relationship between mesolimbic DA release and sniffing behavior. We took advantage of whole-body plethysmography to assess respiratory cycles in awake mice and therefore to identify bouts of sniffing. In this method, breaths are detected by a pressure transducer which accesses the inside of the chamber (**Fig 2A**). The technical needs of our experiments require a patch cable attached to the mouse in the chamber (*e.g.,* **Fig 2C**) which may impair fidelity of the respiratory signal since the cable would need to exit the plethysmography chamber which is normally air-tight. Further, we wished to identify temporal relationships between sniffing and other signals (DA, photostimulation, *etc*) and this mandates that first we establish a temporal relationship between breaths detected with whole-body plethysmography and breathing of mice which occurs only through their noses since they are obligate nasal air breathers. Therefore, we simultaneously monitored respiration via the plethysmograph as well as by means of a chronically-implanted cannula into the dorsal nasal recess of awake mice (**Fig 2A**) (Wesson et al., 2008). For the intranasal measures, a flexible tube was connected to the nasal cannula which passed through the top of the plethysmograph via a snug 3D-printed fitting which allowed for mice to explore and freely-rotate within the plethysmograph (see Supp Materials). The end of this tube terminated into

185 a pressure transducer for amplification of intranasal pressure changes. Using this simultaneous
186 approach, we confirmed that whole body plethysmography, even with the patch cable freely
187 passing through the chamber, reliably detected intranasal respiratory cycles, and faithfully
188 followed during high frequency sniffing bouts (**Fig 2Bi & 2Biii**). The only notable difference we
189 observed for the purpose of this study was a slight temporal lag with the peaks of the whole-body
190 plethysmograph signal trailing those of the intranasal signal (**Fig 2Bii**; lag mean 0.028 ± 0.007s,
191 range 0.01-0.21s; mean of 916 respiratory events from one mouse). This lag is anticipated since
192 the origin of the signal is from within the mouse (intranasal) versus from within a chamber
193 (plethysmograph).
194
195 Having confirmed the ability to accurately detect both individual respiratory cycles and sniffing
196 bouts alike, we next monitored the relationship between DA levels in the ventral striatum as they
197 relate to sniffing. We injected mice into either the medial TuS, the NAcSh, or NAcC with an
198 anterograde AAV encoding $GRAB_{DA}$ (pAAV.hSyn-GRAB_DA1h) (Sun et al., 2018) and in the
199 same surgery implanted into the structure receiving the AAV, a 400μm optical fiber for later fiber
200 photometry. Following several days for surgical recovery, we placed the mice in a plethysmograph
201 for simultaneous monitoring of respiration and DA levels (**Fig 2C**). Since mice rapidly transition
202 in and out of sniffing bouts (Wesson et al., 2008), we restricted our analyses to more
203 stable/pronounced bouts versus short bouts by only defining a sniff bout as the occurrence of
204 sniffing ≥6Hz for ≥1s in duration. Further, in some instances, mice continuously sniff for numerous
205 seconds and then reengage in another bout shortly thereafter. Since these may reflect periods of
206 more generalized arousal versus spontaneous exploratory behavior, we excluded sniff bouts
207 occurring in proximity to these long (>10s) sniffing bouts. We analyzed the relationship between
208 DA levels and sniffing in several manners, and in all analyses, we accounted for the lag between
209 when a nasal inhalation occurs and when the plethysmograph detects the inhalation by subtracting
210 28ms (see **Fig 2Bii**) from the onset event of every peak-detected respiratory cycle.
211
212 We analyzed DA levels across trials wherein mice in the plethysmograph spontaneously sniffed,
213 were delivered a novel odor to evoke sniffing, or were delivered an auditory/somatosensory
214 stimulus by connecting a vibration motor to the plethysmograph which modestly resonated the
215 chamber while simultaneously providing a small auditory 'buzz' cue due to its motor. All mice
216 were confirmed to have implants extending into the mTuS, NAcC, or the NAcSh (**Fig 2D**).
217
218 First, we looked at the relationship between spontaneous sniffing like that displayed by mice
219 during self-motivated states of exploration. As shown in the example traces from a mouse
220 implanted into the TuS (**Fig 2E**), spontaneous sniffing was associated with elevations in the
221 $GRAB_{DA}$ signal. Across mice, $GRAB_{DA}$ levels during spontaneous sniffing were elevated in both
222 the TuS and the NAcSh, but in contrast were decreased in the NAcC (**Fig 2Fi, 2Gi, 2Hi**; TuS
223 paired $t(6)=11.85$ $p<0.0001$; NAcSh paired $t(6)=6.56$, $p=0.0006$; NAcC paired $t(6)=12.15$,
224 $p<0.0001$). Only in the TuS, was the vigor of the spontaneous sniffing bout (the average frequency
225 throughout the bout) correlated with the amplitude of the $GRAB_{DA}$ signal (**Fig 2Fii, 2Gii, & 2Hii;**
226 TuS Pearson's $r(83)=0.29$, $p=0.008$), but not in the NAcSh or NAcC (NAcSh Pearson's
227 $r(101)=0.12$, $p=0.2493$; NAcC Pearson's $r(102)=0.038$, $p=0.703$).
228
229 Next, we investigated the relationship between odor-evoked sniffing and DA levels (**Fig 3A**). As
230 shown in the example in **Figure 3B** from a mouse implanted in the TuS, presentation of a novel

odor was associated with robust increases in sniffing, which was accompanied by an increase in the $GRAB_{DA}$ signal. Across all groups (TuS, NAcSh, NAcC), sniffing frequency was elevated compared to baseline for the first presentation of a novel odor (TuS paired $t(6)=19.23$, $p<0.0001$; NAcSh paired $t(6)=13.27$, $p<0.0001$; NAcC paired $t(6)=14.35$, $p<0.0001$), which habituated across subsequent presentations of the same odor (TuS rmANOVA $F(2.26,13.55)=14.64$, $p=0.0003$; NAcSh rmANOVA $F(2.44, 14.65)=32.65$, $p<0.0001$; NAcC rmANOVA $F(1.59, 9.55)=23.5$, $p=0.0003$) (**Figs 3Ci, 3Di, & 3Ei**). Simultaneously during novel odor-evoked sniffing bouts (trial #1 of odor), we observed elevations in the $GRAB_{DA}$ signal in both the TuS and NAcSh (**Fig 3Cii & 3Dii**; TuS paired $t(6)=6.54$, $p=0.0006$; NAcSh paired $t(6)=4.38$, $p=0.005$). The increases rose soon around sniff bout onset and decayed within a few seconds. In contrast, the NAcC displayed reduction in the $GRAB_{DA}$ signal upon sniffing (**Fig 3Eii**; paired $t(6)=8.35$, $p=0.0002$).

The elevation in the $GRAB_{DA}$ signal was not solely due to odor input since the signal became attenuated across repeated odor deliveries in the TuS and NAcSh **(Fig 3Ciii & 3Diii**; trials #1-5; TuS rmANOVA $F(2.08, 12.48)=7.942$, $p=0.006$; NAcSh rmANOVA: $F(1.90,11.39)=5.563$, $p=0.022$), whereupon trial 5, the $GRAB_{DA}$ signal was observed near baseline levels. In the NAcC, reductions in the $GRAB_{DA}$ signal was not relieved with repeated odor presentations (**Fig Eiii**; rmANOVA $F(1.98, 11.90)=0.5760$, $p=0.58$). Also supporting that the change in amplitude of the $GRAB_{DA}$ signal is related to sniffing, we found that the vigor of odor-evoked sniffing correlated with the peak of the $GRAB_{DA}$ signal in both the TuS and NAcSh (TuS Pearson's $r(34)=0.65$, $p<0.0001$; NAcSh Pearson's $r(34)=0.51$, $p=0.002$), but not in the NAcC (Pearson's $r(34)=-0.14$, $p=0.414$) (**Figs 3Civ, 3Div, & 3Eiv**). Interestingly here, the odor-evoked sniffing in the NAcSh was correlated with $GRAB_{DA}$ levels which was not the case with spontaneous sniffing (**Fig 2G**), suggesting in the NAcSh the relationship may dependent upon odor.

Finally, we assessed the impact of the multimodal buzz stimulus on $GRAB_{DA}$ levels. While not as dramatic nor reliable as an odor (as in **Fig 3Ci, Di, & Ei**), the buzz stimulus evoked sniffing greater than baseline in the majority of mice (**Fig 3Fi, Gi, & Hi**). Correspondingly, DA was elevated upon initial buzz-evoked sniffing in the TuS and the NAcSh (**Figs 3Fii & Gii**; TuS paired $t(6)=6.77$, $p=0.0005$; NAcSh paired $t(6)=3.17$, $p=0.019$). The buzz-evoked sniffing did not strongly habituate across repeated trials, and likewise, $GRAB_{DA}$ levels also remained consistent across trials (**Figs Fi & iii**, **Figs Gi & iii**; TuS sniffing rmANOVA $F(2.57, 15.4)=1.351$, $p=0.293$; TuS $GRAB_{DA}$ rmANOVA $F(1.90, 11.38)=0.49$, $p=0.616$; NAcSh sniffing rmANOVA $F(2.43, 14.58)=2.97$, $p=0.0752$; NAcSh $GRAB_{DA}$ rmANOVA $F(1.32, 7.94)=0.27$, p-0.6786). Interestingly, in the NAcSh, there was a biphasic increase in $GRAB_{DA}$ with the first phase occurring upon buzz onset, and the second upon buzz offset (**Fig 3Gii**). Whereas in the NAcSh, $GRAB_{DA}$ levels measured upon either phase were not correlated with the vigor of sniffing (**Fig 3Giv**; during buzz Pearson's $r(34)=-0.17$, $p=0.316$; upon buzz offset Pearson's $r(34)=-0.074$, $p=0.673$), the $GRAB_{DA}$ levels upon buzz strongly correlated with sniffing vigor in the TuS (**Fig 3Eiv**; Pearson's $r(34)=0.43$, $p=0.011$). Similar to that seen for both spontaneous sniffing and odor-evoked sniffing, $GRAB_{DA}$ levels in the NAcC were reduced upon buzz-evoked sniffing (**Fig 3Hii**; paired $t(6)=3.23$, $p=0.018$) which similarly did not habituate across trials (**Figs 3Hii & 3Hiii**; rmANOVA $F(2.19, 13.14)=0.44$, $p=0.668$). There was no correlation between buzz-evoked sniffing vigor and $GRAB_{DA}$ levels in the NAcC (**Fig 3Hiv**; Pearson's $r(34)=-0.22$, $p=0.194$). When comparing the peak $GRAB_{DA}$ responses across all regions and all conditions, we found similar evoked responses in the TuS and NAcSh to novel odor presentations and during spontaneous sniffing **(Fig 3I**; two-

way ANOVA, main effect of region $F(2,54)=97.73$, $p<0.0001$; Tukey's multiple comparisons TuS vs. NAcSh odor $p=0.99$; TuS vs. NAcSh spont $p=0.469$). Upon first presentation of the buzz, $GRAB_{DA}$ signals in the TuS were higher than in the NAcSh (Tukey's multiple comparisons TuS vs. NAcSh buzz $p=0.006$). Taken together, these results indicate that sniffing corresponds with increases in DA release in two specific sub-regions of the ventral striatum, and that the level of DA correlates to the vigor of sniffing.

DA release into the ventral striatum elicits sniffing

Given the relationship between DA release in the ventral striatum and the occurrence and vigor sniffing, we next sought to determine whether this release of DA is sufficient to elicit sniffing. To assess this, we injected an anterograde Cre-dependent Channelrhodopsin2 (AAV5-EF1α-DIO-hChR2(E123T/T159C)-EYFP) unilaterally into the VTA of DAT^{IRES}-Cre mice (**Fig S2**) and implanted an optical fiber terminating over the TuS, NAcSh, or NAcC to drive terminal release of DA upon light stimulation (**Fig 4A & B**). Control mice were injected with anterograde AAV solely expressing EYFP in the VTA (AAV5-EF1α-DIO-eYFP) and also received an optical fiber terminating over the TuS, NAcSh, or NAcC. One second long, 25Hz 473nm light stimulation was delivered through the optical fiber while mice were in the plethysmograph. This 25Hz stimulus was selected based upon prior work using the same stimulus paradigm to elicit VTA DA release into the ventral striatum (Oettl et al., 2020). As shown in **Figure 4C**, in an example mouse, photostimulation of DAergic terminals in the TuS evoked a brief bout of sniffing. In this example mouse, the average latency to onset of a sniff bout was 240ms ± 22.5ms (across trial range: 130-330ms; bout onset defined as the moment of achieving ≥6Hz respiration). Further, the average amount of time spent sniffing (time ≥6Hz) during photostimulation was 672 ± 59.6ms (across trial range: 310-1000ms). The light evoked sniffing in this example mouse was also reliable across repeated trials (**Fig 4C**).

In all three ChR2-injected groups of mice, we observed a rapid increase in respiratory frequency upon photostimulation (**Fig 4D**). This photostimulation-evoked display of sniffing was largely maintained across repeated trials (**Figs 4D & E;** testing for stability in Hz across trials: mixed-effects analysis $F(4.09, 85.87)=2.34$, $p=0.058$). While anticipated, EYFP control mice displayed a slight increase in respiratory frequency during photostimulation, likely due to the arousing nature of the visual stimulus leaking from the fiber implant. Though the frequency of the sniffing bout was lower in EYFP mice than in all ChR2-treated groups (**Fig 4D, right, Fig 4E & F**). As shown in **Figure 4F**, the temporal dynamics of photostimulation-evoked sniffing in ChR2-injected mice was remarkedly similar. The average latency to onset of a sniff bout was 279.4 ± 13.3ms SEM (inter-mouse range: 225-362.5ms) for TuS, 264.7 ± 14.83ms SEM (inter-mouse range: 202.5-299ms for NAcSh, and 263.3 ± 7.52ms SEM (inter-mouse range: 242.2-290ms) for NAcC (**Fig 4Gi**). Further, the average amount of time spent sniffing during photostimulation was 534.1 ± 37.8ms (inter-mouse range 314.3-743ms) for TuS, 647.7 ± 53.7ms (inter-mouse range 479 – 834ms) for NAcSh, and 520.1 ± 85.7ms (inter-mouse range 254.4 - 755ms) for NAcC. All ChR2-treated mice spent more time sniffing than EYFP controls, and there were no significant differences between ChR2-treated groups (**Fig 4Gii**) (one-way ANOVA $F(3,28)=14.02$, $p<0.0001$; Tukey's multiple comparisons test TuS vs. EYFP $p=0.0001$, NAcSh vs EYFP $p<0.0001$, NAcC vs EYFP $p=0.0017$). Further, the vigor of photostimulation-evoked sniffing (measured as the peak Hz during photostimulation) did not differ between ChR2-treated groups and was significantly greater than EYFP controls (**Fig 4Giii**; one-way ANOVA $F(3, 28)=14.17$,

323 $p<0.0001$; Tukey's multiple comparisons test TuS vs. EYFP $p<0.0001$, NAcSh vs. EYFP
324 $p<0.0001$; NAcC vs. EYFP $p=0.0010$). Finally, we explored the reliability whereby a DAergic
325 terminal photostimulation would elicit a sniffing bout. The probability that photostimulation
326 elicited sniffing was robust, and significantly greater than in EYFP controls – indeed with many
327 animals in each ChR2-treatment group displaying a sniff bout to *every* photostimulation trials and
328 the vast majority to >80% of trials (**Fig 4Giv**; one-way ANOVA $F(3, 28)=11.01$, $p<0.0001$;
329 Tukey's multiple comparisons TuS vs. EYFP $p=0.0002$, NAcSh vs. EYFP $p=0.0002$, NAcC vs.
330 EYFP $p=0.004$).
331
332 Since VTA neurons are known to co-release glutamate in addition to dopamine (Sulzer et al., 1998;
333 Hnasko et al., 2010; Stuber et al., 2010), and knowing that ventral striatum neurons express
334 glutamatergic receptors, we next sought to isolate the influence of the above effect (**Fig 4**) on DA
335 versus glutamate. We crossed *VGluT2 fl/fl* mice with mice expressing Cre recombinase in all cells
336 expressing tyrosine hydroxylase (*TH-Cre*), the rate-limiting enzyme upstream for DA synthesis.
337 As above, we injected *VGluT2fl/fl* x *TH-Cre* mice with the same ChR2-expressing virus or
338 associated control virus unilaterally into the VTA and implanted an optical fiber terminating over
339 the TuS to drive terminal excitation. Since photostimulation in all three ventral striatum subregions
340 of ChR2-expressing mice in the prior experiment drove sniffing, here we excluded the NAcC
341 group for simplicity. As shown in **Figure S3**, photostimulation of DAergic terminals in *VGluT2fl/fl*
342 x *TH-Cre* mice elicited sniffing with comparable temporal dynamics, vigor, and probability as in
343 *DAT-Cre* mice (**see Fig 4**) and at greater amounts in *VGluT2fl/fl* x *TH-Cre* mice than in EFYP
344 controls.
345
346 We next wanted to determine whether DA release in the ventral striatum serves to 'initiate'
347 sniffing, or if it further can persistently drive sniffing over extended time courses. To test this, in
348 the same ChR2-treated DAT^{IRES}-Cre mice as in **Figures 4B-G,** we delivered repeated
349 presentations of the 25Hz photostimulation for either 120ms, 1s, 2s, or 4s. We predicted that if DA
350 initiates sniffing we would see transiently-evoked sniffing across all stimulation durations,
351 whereas if DA drives sniffing, we would see the duration of sniffing bouts would track the duration
352 of the photostimulation. As shown in **Figure 4H**, we found that the dynamics of the sniffing bout
353 was equivalent regardless of photostimulation duration. Indeed, in all three ChR2-treated groups,
354 photostimulation of DAergic terminals elicited a statistically similar sniffing vigor (TuS mixed-
355 effects analysis; $F(1.78, 6.53)=0.94$ $p=0.426$; NAcSh rmANOVA $F(1.63, 4.89)=0.924$, $p=0.436$;
356 NAcC rmANOVA $F(1.93, 5.79)=0.24$, $p=0.789$), and similar percentage of time sniffing (TuS
357 mixed-effects analysis $F(1.18, 4.32)=1.57$, $p=0.284$; NAcSh rmANOVA $F(1.50, 4.5)=0.77$
358 $p=0.479$; NAcC rmANOVA $F(1.43, 4.30)=1.81$, $p=0.404$). These results indicate that DA release
359 into the ventral striatum initiates sniffing, but that it does not persistently driving a sniff bout.
360
361 Stimulation of respiratory brain stem regions known to support breathing can generate sniffing
362 patterns even in anesthetized mice (*e.g.,* (Del Negro et al., 2018; Ramirez and Baertsch, 2018; Liu
363 et al., 2022)). Is mesolimbic DA input to the ventral striatum capable of initiating sniffing even in
364 anesthetized mice? To test this, following the above experiments, DAT^{IRES}-Cre mice injected with
365 ChR2 were deeply anesthetized with urethane and photostimulation was delivered (see Supp
366 Materials). The baseline respiratory pattern and rate in these mice were both stable and slow
367 (<1.25Hz), indicating deep sedation. Breathing rate under anesthesia showed no change upon
368 photostimulation of DAergic terminals in either the TuS or the NAcSh and NAcC (**Fig 5A - C**),

suggesting that the VTA→ventral striatum DAergic circuit is a component of the voluntary, not automatic, respiration-control system.

Sniffing bouts can be displayed in response to a variety of stimuli an animal may perceive in its environment. While not well-studied, it is possible the temporal dynamics of sniffing bouts may differ based upon what elicited the sniffing. We wanted to know if the sniffing bouts triggered by DA release into the ventral striatum are similar, or distinct from, those which are elicited in response to a stimulus or those bouts spontaneously generated? To address this, we used a machine learning approach (**Fig 5D;** see Supp Materials). We converted 1s long sniffing traces (the 1s following bout onset) into 1sec long instantaneous sniffing frequency arrays (10ms bin size). Next, we used K-nearest neighbors with Diffusion Time Warping (DTW) (Sakoe and Chiba, 1978; Bagnall et al., 2017; Regan, 2018) to calculate the difference in sniffing frequency dynamics between frequency arrays. With DTW, the smaller the value reported in each time bin corresponds to the dynamics between arrays being more similar at that moment. The model was trained on DTW arrays from odor-evoked, spontaneously-generated, and photostimulation-evoked data (n=63-70 arrays/group). Following, we fed the model DTW arrays from each group to test how distinct the sniffing dynamics are between groups. We found that photostimulation-evoked sniffing was highly distinct from all other types of sniffing, with >84% correct classification (**Fig 5E**). This is comparable to the accuracy of classifying odor-evoked sniffing, which is known to be highly stereotyped (84%, **Fig 5E**). As a comparison, spontaneously evoked sniffing was only accurately classified ~38% of the time, likely due to the variability in these self-motivated bouts. This result implies that DA release into the ventral striatum engages a distinct respiratory pattern from that when an animal engages in self-motivated exploration or upon perception of an environmental stimulus (*i.e.*, an odor).

Sniffing recruits ventral striatum neurons

VTA DA is released onto spiny projection neurons in the ventral striatum expressing either the D1 or D2 DA receptor. Are these neurons recruited upon sniffing? To test this, we injected a Cre-dependent anterograde AAV expressing GCamP6f (AAV.Syn.Flex.GCaMP6f.WPRE.SV40) into the TuS of D1-Cre and D2-Cre mice (Gong et al., 2007) which also were subsequently implanted with a 400µm core optical fiber over the TuS (**Fig 6A & B**). To limit movement artifacts and to allow optimal control of the snout's position for receipt of an odor, the mice were also implanted with a head-bar for later head-fixation. An extra-nasal flow sensor was positioned near the animal's nose to monitor sniffing (Jordan et al., 2018). We analyzed D1 and D2 neuron activity across trials wherein mice spontaneously entered into bouts of sniffing and also during novel odor-evoked sniffing.

Similar to that observed with DA release into the ventral striatum (**Fig 2**), the activity of both D1 and D2 neurons increased upon spontaneous sniffing bouts (**Fig 6C**). D1 and D2 neuron evoked responses were comparable in their temporal dynamics, and both groups displayed similar evoked sniffing vigor (**Fig 6C**; unpaired $t(16)=1.084$, $p=0.294$). The activity of D2 neurons also positively correlated with the vigor of spontaneous sniffing (**Fig 6Civ & Cv**)(D1 Pearson's $r(37)=0.19$, $p=0.241$; D2 Pearson's $r(68)=0.48$, $p<0.0001$).

Novel odor delivery evoked sniffing in both D1- and D2-Cre mice (paired $t(11)=11.58$, $p<0.0001$), which habituated across subsequent presentations of the same odor (**Fig 6Di**) (rmANOVA $F(1.73, 19.07)=35.82$, $p<0.0001$). During novel odor-evoked sniffing bouts, D1 and D2 neurons increased in their activity (**Fig 6Dii & Div)**; D1-Cre: paired $t(9)=7.03$, $p<0.0001$; D2-Cre: paired $t(9)=9.88$,

$p<0.0001$). Reminiscent of changes in DA release across repeated trials of odor-evoked sniffing (**Fig 3**), the activity of D1 and D2 neurons similarly reduced across repeated presentations (**Fig 6Diii & v**; D1-Cre: rmANOVA $F(1.42, 12.77)=15.69$, $p=0.0008$; D2-Cre: rmANOVA $F(1.80, 16.21)=25.01$ $p<0.0001$). The evoked neural activity and its subsequent adaptation across trials was similar in D1- and D2 mice (**Fig 6vi**; two-way ANOVA, no effect of genotype $F(1, 18)=1.387$, $p=0.254$). These results indicate that DA receptor-expressing ventral striatum neurons post-synaptic from midbrain DAergic terminals are recruited upon bouts of sniffing.

DA receptor antagonism in the ventral striatum reduces both the occurrence and vigor of sniffing

Ventral striatum neural activity can be influenced by a wealth of neurotransmitters/neuromodulators arising from numerous bottom-up and top-down brain regions. For instance, NAc activity is influenced not only by DA, but also by glutamatergic inputs from the frontal cortex (Scofield et al., 2016). While the above results suggest that sniff-evoked changes in mesolimbic DA influx to the ventral striatum engages postsynaptic neurons, those results still beg the question: is DA binding to DA receptors on ventral striatum neurons needed for an animal to initiate sniffing?

We implanted C57BL/6J mice of both sexes with bilateral indwelling infusion cannulae into either their NAcSh or TuS (**Fig 7A**). We focused on antagonism of DA receptors in the TuS and NAcSh since it was within these regions wherein we found the strongest correlation between DA levels and sniffing vigor (**Figs 3 & 4**). Since TuS and NAcSh neurons may express D1, D2, or D3 receptors (Bouthenet et al., 1991; Mansour et al., 1991; Le Moine and Bloch, 1995; Cepeda et al., 2008; Zhang et al., 2021), across days in a counter-balanced within subject's design, each mouse was intracranially infused with SCH23390, raclopride, or PG01037 to selectively inhibit D1, D2, or D3 receptors, respectively (see Supp Materials). The infusion occurred 10min prior to placing the mouse into the plethysmograph for respiratory monitoring, wherein we measured both spontaneous and sensory-evoked sniffing bouts (**Fig 7B)**. We analyzed for effects of D1, D2, and D3 antagonism on both the number of sniff bouts and their vigor, displayed spontaneously and stimulus-evoked.

We found that D1 receptor binding contributed to spontaneous sniffing in that D1 receptor antagonism in the TuS reduced the number of spontaneous sniffing bouts (**Fig 7Ci;** two-way ANOVA, main effect of treatment $F(1, 24)=12.62$, $p=0.002$; Sidak's multiple comparisons TuS VEH vs. SCH $p=0.023$). D1 receptor binding also contributed to sensory-evoked sniffing in that D1 receptor antagonism in the TuS reduced the number of buzz-evoked bouts (**Fig 7Ei**; two-way ANOVA, main effect of treatment $F(1, 24)=4.30$, $p=0.049$; Sidak's multiple comparisons TuS VEH vs. SCH $p=0.048$).

Likewise, we found that D2 receptor binding contributed to spontaneous sniffing in that D2 receptor antagonism in both the TuS and NAc reduced the number and vigor of spontaneous sniffing bouts (**Fig 7Cii**; two-way ANOVA, main effect of treatment $F(1, 24)=48.64$, $p<0.0001$; Sidak's multiple comparisons TuS VEH vs RAC $p<0.0001$, NAc VEH vs RAC $p=0.002$). D2 receptor binding in the TuS and NAc also contributed to odor-evoked sniffing in that D2 receptor antagonism reduced the number of sniffing bouts (**Fig 7Dii**; two-way ANOVA, main effect of

treatment $F(1, 24)=31.26$, $p<0.0001$; Sidak's multiple comparisons TuS VEH vs RAC $p<0.0001$, NAc VEH vs RAC $p=0.017$. In contrast, we saw no effect of D3 receptor inhibition on spontaneous or odor-evoked sniffing in either the TuS or NAcSh (**Fig 7Ciii, 7Diii, 7Eiii**).

Interestingly, D2 antagonism in both the TuS and NAc not only reduced the number of odor-evoked bouts displayed by mice, but in both regions, the odor-evoked bouts which were displayed were reduced in vigor (**Fig S4Bi & 4Bii**; D1 two-way rmANOVA main effect of treatment $F(1, 24)=7.75$, $p=0.010$; Sidak's multiple comparisons TuS VEH vs. SCH $p=0.228$, NAcSh VEH vs. SCH $p=0.056$; D2 two-way rmANOVA, main effect of treatment $F(1, 24)=96.64$, $p<0.0001$; Sidak's multiple comparisons TuS VEH vs. RAC $p<0.0001$, NAcSh VEH vs. RAC $p<0.0001$). This was not observed during spontaneous sniffing bouts or buzz-evoked sniffing bouts pointing to a unique system which supports the vigor of odor-evoked sniffing compared to spontaneous sniffing which was influenced solely in terms of the total number of bouts. Altogether, these results confirm that mesolimbic DA initiates sniffing by its actions upon D1 and D2 receptors in the TuS and NAcSh.

Discussion

DA appears to partake in numerous functions (Wise, 2004; Morales and Margolis, 2017; Berke, 2018; Markowitz et al., 2023). For instance, DA can influence the perceived salience of stimuli wherein DA might make certain smells stand out more (Zhang et al., 2017), making them more noticeable during sniffing. DA might enhance our sensitivity to sensory stimuli, including odors, allowing them to be better detected at low levels (Ennis et al., 2001). DA is also involved in arousal and attention mechanisms wherein it could heighten our alertness and focus on sensory inputs, including odors and other cues (Nieoullon, 2002; Bromberg-Martin et al., 2010). Further, DA is involved in synaptic plasticity and learning from experiences and adapting to new information. When sniffing odors, DA release, including upon ventral striatum neurons, could contribute to the brain's ability to form associations and learn information (Wieland et al., 2015). Likewise, when we encounter pleasant or novel odors, DA release might contribute to feelings of pleasure and satisfaction (Midroit et al., 2021). Indeed, DA is a key transmitter in the brain's reward system and is connected to motivation and exploration (Legault and Wise, 2001), wherein it may influence our motivation to sniff, encouraging us to explore and investigate different odor landscapes. Furthermore, several lines of evidence have documented the orchestration of sniffing during motivated behaviors and even upon anticipation of a reinforcer. These functions of DA stated, no prior work has linked DA with the highly conserved and ethologically-relevant behavior of sniffing. Our results support a model wherein DA acts upon the ventral striatum, specifically upon neurons with D1 and D2 receptors in the TuS and NAcSh, to both initiate and invigorate sniffing. We predict the promotion of sniffing by DA is an essential component linking the historic cooccurrence of sniffing with motivated states.

Stimulus active sampling behaviors have a tight linkage to both the acquisition and processing of environmental information, and these are modulated by ascending monoaminergic neurotransmission. For instance, stimulation of the locus coeruleus in rats increases the responsiveness of barrel cortex neurons to whisker deflection (Motaghi et al., 2006). In zebra

finches, auditory coding in the finch auditory cortex homologue is modulated by norepinephrine (Lee et al., 2018). Likewise, visual processing in the lateral geniculate nucleus of cats is modulated by dopamine (Zhao et al., 2002). In terms of active sampling behaviors and their regulation by monoaminergic transmission, rhythmic licking in mice can be suppressed by DA D1 receptor antagonism in the motor cortex (Chen et al., 2019). The rhythmic movement of the vibrissae within ('whisking') is perhaps the most well-studied in terms of its modulation by monoaminergic inputs. Serotonergic input from the dorsal raphe nucleus, whose neurons fire rhythmically within the whisking frequency bands, generates whisking in rats and whisking can be diminished by serotonin receptor antagonism in the dorsal raphe (Hattox et al., 2003). Also, recent evidence indicates that mesolimbic DA input to the NAc in mice promotes orofacial behaviors including whisking (Li et al., 2023). Our results add to these prior studies by establishing a necessary and sufficient role for mesolimbic DA in the initiation of sniffing behavior in that not only does photostimulation of DAergic terminals initiate sniffing bouts, but also, blockade of DAergic receptors suppresses the normal occurrence of sniffing and its vigor. In line with these results, VTA→ventral striatum DA may serve as a pathway to facilitate adaptive sniffing to promote olfactory search behavior, and moreover may shape odor processing given the regulation of odor coding and perception by the respiratory rhythm (Cury and Uchida, 2010; Shusterman et al., 2011; Iwata et al., 2017).

We found heterogeneity of DA release in ventral striatum subregions. This finding is reminiscent of those monitoring DA release during other behaviors which has uncovered heterogeneous levels of DA in the NAcC versus NacSh in manners likely supported by differing VTA neural pathways innervating these subregions (Badrinarayan et al., 2012; Beier et al., 2015; Yang et al., 2018). Here we found that in comparison to the increases in DA upon sniffing in both the TuS and NAcSh, that the NAcC experienced reductions in DA release (**Figs 2 & 3**). This implies that sniffing increases tonic firing of VTA DAergic neurons, or suppresses firing of DAergic neurons, in the NAcSh and TuS and NAcC, respectively. That optical excitation of the terminals in any of the regions equally initiates sniffing suggests that this is overriding changes in VTA neuron firing which give rise to DA dynamics in the ventral striatum and also hints that heterogeneity in subregion DA dynamics are not a byproduct of interregional differences in DA clearance (*e.g.,* by different kinetics or function of the dopamine transporter). It is tempting to speculate that different DA dynamics in these subregions might stem from unique inputs from areas that may signal salience or arousal which would synapse on VTA GABAergic neurons, including projections from the TuS and NAc themselves (Yang et al., 2018).

What 'type' of sniffing does mesolimbic DA initiate? The machine learning model trained on different experimenter classified sniffing patterns (**Fig 5D**) points to mesolimbic DA-evoked sniffing its own type of sniffing, unique from that a mouse would self-motivate upon the desire to explore (spontaneous) and that evoked by a sensory stimulus (like an odor or buzz). So, what type is it? Sniffing is a dynamic behavior which can be displayed in unique manners based upon context. For instance, dogs sniff at lower frequencies when searching the air for odors than when searching on the ground wherein they elevate their sniffing rate (Steen et al., 1996). Rats also display sniffing in a distinct frequency band when transitioning from sampling odors to anticipating a reinforcer in an instrumental task in manners which suggests sniffing reflects strategic 'modes' or states (Kepecs et al., 2007). Our results are in-line with these prior works and suggest that mesolimbic DA-evoked sniffing reflects a unique sniffing mode. Several reports have established links between specific brain regions, and neurons within those brain regions, in regulating adaptive

553 respiration, although the role of those regions does not appear to initiate sniffing as much as shape
554 more specific respiratory parameters (*e.g.,* (Angelakos et al., 2023). Our results wherein we varied
555 photostimulation of DAergic terminals uncovered that the duration of evoked-sniffing bouts did
556 not increase with more prolonged optical stimulation (**Fig 4H**). This suggests that DA release into
557 the ventral striatum is more so to initiate and possibly invigorate sniffing than to maintain its tonic
558 display.
559
560 There are a few caveats to this study we believe important to note. First, optogenetic stimulation
561 of DAergic terminals, while herein an effective means at robustly driving sniffing, is likely driving
562 DA release onto postsynaptic neurons in supraphysiological manners. While we selected a
563 stimulation paradigm established by others to be effective on TuS projecting VTA terminals, it is
564 nevertheless likely DA is released at higher than usual levels. Nevertheless, both our
565 pharmacological data (**Fig 7**) and our work wherein we removed *VGluT* from tyrosine hydroxylase
566 expressing neurons (**Fig S3**) all agree that DA is contributing to the initiation of sniffing. It is also
567 possible that some behavioral effects from the photostimulation are due to backpropagation of
568 activity into the VTA itself. Again though, the pharmacological results indicate DA input to the
569 ventral striatum is important for sniffing. Second, while DA release into the VS initiates sniffing,
570 and while in several of our analyses DA levels were correlated with vigor of sniffing frequency,
571 this was not always the case. For instance, for the buzz stimulus experiments, large DA levels were
572 found despite the mice only displaying modest frequencies of sniffing. This corresponds with other
573 studies which have reported DA release in response to a variety of salient stimuli. Finally, while
574 D2 receptors are enriched on spiny projection neurons in the TuS and NAc, they also serve
575 autoreceptor functions on VTA DAergic terminals, including those innervating these regions. So,
576 while we know local D1 antagonism suppressed sniffing, it is possible the effects of D2 antagonism
577 is due to contributions of antagonizing D2 receptors on both the VTA terminals (which would
578 suppress DA release) and on spiny projection neurons.
579
580 A major question is how the receipt of DA upon spiny projection neurons, and their recipient upon
581 sniffing, might ultimately drive changes in the respiratory rhythm. Both the TuS and NAc have
582 outputs into downstream structures important for homeostatic regulation/control and limbic
583 function. Ventral striatum spiny projection neurons also feedback upon the VTA in manners
584 regulating DA release and this too could support, even if just bisynaptically, modulation of
585 respiratory central pattern generators which are sensitive to dopamine (Sugita et al., 2015; Jhang
586 et al., 2023). Perhaps one clue may reside from our results wherein we attempted to stimulate
587 sniffing under anesthesia and found that DA release into the TuS or NAc is incapable of initiating
588 sniffing (**Fig 5A & B**). This suggests that the functional 'sniffing' output from the ventral striatum
589 is within a structure which can drive changes in breathing but not under anesthesia. It is not
590 uncommon for stimulation of some respiratory control centers to be incapable of altering
591 respiration under anesthesia (Arthurs et al., 2023; Jhang et al., 2023). For instance, the ventral
592 striatum projects to hypothalamic nuclei that are known to innervate respiratory control nuclei in
593 the respiratory pons and could support entrainment of breathing at sniffing frequencies.
594 Interestingly, these hypothalamic targets are also state dependent in that changes in breathing
595 frequency do not occur upon stimulation under anesthesia (Arthurs et al., 2023). Thus, there seems
596 to be somewhat of a paradox in that in some respiratory structures, including the PreBötzinger
597 complex, high frequency stimulation is incapable of driving respiration at frequencies greater than
598 6Hz (Vann et al., 2018; de Sousa Abreu et al., 2022). Identifying what downstream circuits links

599 the TuS and NAc to respiratory brain stem circuits to orchestrate sniffing remains an important
600 goal. Our results point to D1 and D2 ventral striatum neurons being part of a feedforward/feedback
601 loop between the basal ganglia and respiratory control regions with DAergic VTA neurons being
602 an intermediary circuit node.
603
604 In conclusion, we report herein evidence that mesolimbic DA input into the ventral striatum
605 contributes to the display of the widely conserved behavior of sniffing. The nature of sniffing being
606 integral to both olfaction and motivated behaviors implicates this circuit in a wide array of
607 functions.
608
609
610
611
612 **References**

613 Angelakos CC, Girven KS, Liu Y, Gonzalez OC, Murphy KR, Jennings KJ, Giardino WJ, Zweifel LS,
614 Suko A, Palmiter RD, Clark SD, Krasnow MA, Bruchas MR, de Lecea L (2023) A cluster of
615 neuropeptide S neurons regulates breathing and arousal. Current Biology 33:5439-5455.e7.
616 Arthurs JW, Bowen AJ, Palmiter RD, Baertsch NA (2023) Parabrachial tachykinin1-expressing neurons
617 involved in state-dependent breathing control. Nat Commun 14:963.
618 Ashhad S, Kam K, Del Negro CA, Feldman JL (2022) Breathing Rhythm and Pattern and Their Influence
619 on Emotion. Annu Rev Neurosci 45:223–247.
620 Bäckman CM, Malik N, Zhang Y, Shan L, Grinberg A, Hoffer BJ, Westphal H, Tomac AC (2006)
621 Characterization of a mouse strain expressing Cre recombinase from the 3′ untranslated region of
622 the dopamine transporter locus. genesis 44:383–390.
623 Badrinarayan A, Wescott SA, Vander Weele CM, Saunders BT, Couturier BE, Maren S, Aragona BJ
624 (2012) Aversive Stimuli Differentially Modulate Real-Time Dopamine Transmission Dynamics
625 within the Nucleus Accumbens Core and Shell. The Journal of Neuroscience 32:15779–15790.
626 Bagnall A, Lines J, Bostrom A, Large J, Keogh E (2017) The great time series classification bake off: a
627 review and experimental evaluation of recent algorithmic advances. Data Min Knowl Discov
628 31:606–660.
629 Beier KT, Steinberg EE, DeLoach KE, Xie S, Miyamichi K, Schwarz L, Gao XJ, Kremer EJ, Malenka
630 RC, Luo L (2015) Circuit Architecture of VTA Dopamine Neurons Revealed by Systematic Input-
631 Output Mapping. Cell 162:622–634.
632 Berke JD (2018) What does dopamine mean? Nat Neurosci 21:787–793.
633 Bouthenet ML, Souil E, Martres MP, Sokoloff P, Giros B, Schwartz JC (1991) Localization of dopamine
634 D3 receptor mRNA in the rat brain using in situ hybridization histochemistry: comparison with
635 dopamine D2 receptor mRNA. Brain Res 564:203–219.
636 Bromberg-Martin ES, Matsumoto M, Hikosaka O (2010) Dopamine in Motivational Control: Rewarding,
637 Aversive, and Alerting. Neuron 68:815–834.
638 Catania KC (2006) Olfaction: Underwater "sniffing" by semi-aquatic mammals. Nature 444:1024–1025.
639 Cepeda C, André VM, Yamazaki I, Wu N, Kleiman-Weiner M, Levine MS (2008) Differential
640 electrophysiological properties of dopamine D1 and D2 receptor-containing striatal medium-sized
641 spiny neurons. European Journal of Neuroscience 27:671–682.
642 Chen K, Vincis R, Fontanini A (2019) Disruption of Cortical Dopaminergic Modulation Impairs
643 Preparatory Activity and Delays Licking Initiation. Cerebral Cortex 29:1802–1815.
644 Clarke S, Trowill JA (1971) Sniffing and motivated behavior in the rat. Physiol Behav 6:49–52 Available
645 at:
646 http://www.ncbi.nlm.nih.gov/entrez/query.fcgi?cmd=Retrieve&db=PubMed&dopt=Citation&list_ui
647 ds=4942174.

Cury KM, Uchida N (2010) Robust Odor Coding via Inhalation-Coupled Transient Activity in the Mammalian Olfactory Bulb. Neuron 68:570–585 Available at: http://www.sciencedirect.com/science/article/B6WSS-51CSGBM-S/2/c65fe51eeb2b93b98400aad0d6f20c1a.

Del Negro CA, Funk GD, Feldman JL (2018) Breathing matters. Nat Rev Neurosci 19:351–367.

de Sousa Abreu RP, Bondarenko E, Feldman JL (2022) Phase- and state-dependent modulation of breathing pattern by preBötzinger complex somatostatin expressing neurons. J Physiol 600:143–165.

Ennis M, Zhou F-M, Ciombor KJ, Aroniadou-Anderjaska V, Hayar A, Borrelli E, Zimmer LA, Margolis F, Shipley MT (2001) Dopamine D2 receptor-mediated presynaptic inhibition of olfactory nerve terminals. J Neurophysiol 86:2986–2997.

Floresco SB (2015) The Nucleus Accumbens: An Interface Between Cognition, Emotion, and Action. Annu Rev Psychol 66:25–52.

Gadziola MA, Stetzik LA, Wright KN, Milton AJ, Arakawa K, del Mar Cortijo M, Wesson DW (2020) A neural system for encoding the association of odors with rewarded outcomes and promoted behavioral engagement. Cell Rep 32:107919.

Gong S, Doughty M, Harbaugh CR, Cummins A, Hatten ME, Heintz N, Gerfen CR (2007) Targeting Cre Recombinase to Specific Neuron Populations with Bacterial Artificial Chromosome Constructs. The Journal of Neuroscience 27:9817 LP – 9823.

Haber SN (2011) Neuroanatomy of Reward: A View from the Ventral Striatum (Gottfried JA, ed). Boca Raton (FL): CRC Press.

Hattox A, Li Y, Keller A (2003) Serotonin Regulates Rhythmic Whisking. Neuron 39:343–352.

Hnasko TS, Chuhma N, Zhang H, Goh GY, Sulzer D, Palmiter RD, Rayport S, Edwards RH (2010) Vesicular glutamate transport promotes dopamine storage and glutamate corelease in vivo. Neuron 65:643–656.

Ikemoto S (2003) Involvement of the Olfactory Tubercle in Cocaine Reward: Intracranial Self-Administration Studies. The Journal of neuroscience 23:9305–9311.

Ikemoto S (2007) Dopamine reward circuitry: Two projection systems from the ventral midbrain to the nucleus accumbens-olfactory tubercle complex. Brain Res Rev 56:27–78.

Ikemoto S, Panksepp J (1994) The relationship between self-stimulation and sniffing in rats: does a common brain system mediate these behaviors? Behav Brain Res 61:143–162 Available at: http://www.ncbi.nlm.nih.gov/pubmed/8037862?ordinalpos=1&itool=EntrezSystem2.PEntrez.Pubmed.Pubmed_ResultsPanel.Pubmed_RVAbstractPlus.

Isles AR, Baum MJ, Ma D, Keverne EB, Allen ND (2001) Urinary odour preferences in mice. Nature 409:783–784.

Iwata R, Kiyonari H, Imai T (2017) Mechanosensory-Based Phase Coding of Odor Identity in the Olfactory Bulb. Neuron 96:1139-1152.e7.

Jhang J, Liu S, O'Keefe DD, Han S (2023) A top-down slow breathing circuit that alleviates negative affect. bioRxiv.

Jordan R, Kollo M, Schaefer AT (2018) Sniffing Fast: Paradoxical Effects on Odor Concentration Discrimination at the Levels of Olfactory Bulb Output and Behavior. eNeuro 5:ENEURO.0148-18.2018.

Kepecs A, Uchida N, Mainen ZF (2007) Rapid and precise control of sniffing during olfactory discrimination in rats. J Neurophysiol 98:205–213 Available at: http://www.ncbi.nlm.nih.gov/entrez/query.fcgi?cmd=Retrieve&db=PubMed&dopt=Citation&list_uids=17460109.

Kleinfeld D, Deschênes M, Ulanovsky N (2016) Whisking, Sniffing, and the Hippocampal θ-Rhythm: A Tale of Two Oscillators. PLoS Biol 14.

Lammel S, Ion DI, Roeper J, Malenka RC (2011) Projection-Specific Modulation of Dopamine Neuron Synapses by Aversive and Rewarding Stimuli. Neuron 70:855–862 Available at: http://dx.doi.org/10.1016/j.neuron.2011.03.025.

Lee V, Pawlisch BA, Macedo-Lima M, Remage-Healey L (2018) Norepinephrine enhances song responsiveness and encoding in the auditory forebrain of male zebra finches. J Neurophysiol 119:209–220.

Legault M, Wise RA (2001) Novelty-evoked elevations of nucleus accumbens dopamine: Dependence on impulse flow from the ventral subiculum and glutamatergic neurotransmission in the ventral tegmental area. European Journal of Neuroscience 13:819–828.

Le Moine C, Bloch B (1995) D1 and D2 dopamine receptor gene expression in the rat striatum: Sensitive cRNA probes demonstrate prominent segregation of D1 and D2 mRNAS in distinct neuronal populations of the dorsal and ventral striatum. J Comp Neurol 355:418–426.

Liu S, Ye M, Pao GM, Song SM, Jhang J, Jiang H, Kim J-H, Kang SJ, Kim D-I, Han S (2022) Divergent brainstem opioidergic pathways that coordinate breathing with pain and emotions. Neuron 110:857-873.e9.

Li W-R, Nakano T, Mizutani K, Matsubara T, Kawatani M, Mukai Y, Danjo T, Ito H, Aizawa H, Yamanaka A, Petersen CCH, Yoshimoto J, Yamashita T (2023) Neural mechanisms underlying uninstructed orofacial movements during reward-based learning behaviors. Current Biology.

Lobo MK, Nestler EJ (2011) The Striatal Balancing Act in Drug Addiction: Distinct Roles of Direct and Indirect Pathway Medium Spiny Neurons. Front Neuroanat 5:41.

Madisen L, Zwingman TA, Sunkin SM, Oh SW, Zariwala HA, Gu H, Ng LL, Palmiter RD, Hawrylycz MJ, Jones AR, Lein ES, Zeng H (2010) A robust and high-throughput Cre reporting and characterization system for the whole mouse brain. Nat Neurosci 13:133–140.

Mansour A, Meador-Woodruff JH, Zhou Q-Y, Civelli O, Akil H, Watson SJ (1991) A comparison of D1 receptor binding and mRNA in rat brain using receptor autoradiographic and in situ hybridization techniques. Neuroscience 45:359–371.

Markowitz JE, Gillis WF, Jay M, Wood J, Harris RW, Cieszkowski R, Scott R, Brann D, Koveal D, Kula T, Weinreb C, Osman MAM, Pinto SR, Uchida N, Linderman SW, Sabatini BL, Datta SR (2023) Spontaneous behaviour is structured by reinforcement without explicit reward. Nature 614:108–117.

Martin-Lopez E, Xu C, Liberia T, Meller SJ, Greer CA (2019) Embryonic and postnatal development of mouse olfactory tubercle. Molecular and Cellular Neuroscience 11:82–96.

Menegas W, Babayan BM, Uchida N, Watabe-Uchida M (2017) Opposite initialization to novel cues in dopamine signaling in ventral and posterior striatum in mice. Elife 6:e21886.

Midroit M, Chalençon L, Renier N, Milton A, Thevenet M, Sacquet J, Breton M, Forest J, Noury N, Richard M, Raineteau O, Ferdenzi C, Fournel A, Wesson DW, Bensafi M, Didier A, Mandairon N (2021) Neural processing of the reward value of pleasant odorants. Current Biology 31:1592–1605 Available at: https://www.sciencedirect.com/science/article/pii/S0960982221001317.

Mingote S, Chuhma N, Kusnoor S V., Field B, Deutch AY, Rayport S (2015) Functional Connectome Analysis of Dopamine Neuron Glutamatergic Connections in Forebrain Regions. Journal of Neuroscience 35:16259–16271.

Moberly AH, Schreck M, Bhattarai JP, Zweifel LS, Luo W, Ma M (2018) Olfactory inputs modulate respiration-related rhythmic activity in the prefrontal cortex and freezing behavior. Nat Commun 9:1528.

Mogenson G, Jones D, Yim C (1980) From motivation to action: Functional interface between the limbic system and the motor system. Prog Neurobiol 14:69–97 Available at: http://www.sciencedirect.com/science/article/pii/0301008280900180.

Moore JD, Deschenes M, Furuta T, Huber D, Smear MC, Demers M, Kleinfeld D (2013) Hierarchy of orofacial rhythms revealed through whisking and breathing. Nature advance on.

Morales M, Margolis EB (2017) Ventral tegmental area: cellular heterogeneity, connectivity and behaviour. Nat Rev Neurosci 18:73–85.

Motaghi S, Sheibani V, Farazifard R, Joneidi H (2006) Electrical stimulation of locus coeruleus strengthens the surround inhibition in layer V barrel cortex in rat. Neurosci Lett 401:280–284 Available at: https://linkinghub.elsevier.com/retrieve/pii/S0304394006002977.

Murata K, Kanno M, Ieki N, Mori K, Yamaguchi M (2015) Mapping of Learned Odor-Induced Motivated Behaviors in the Mouse Olfactory Tubercle. The Journal of Neuroscience 35:10581–10599.
Nieoullon A (2002) Dopamine and the regulation of cognition and attention. Prog Neurobiol 67:53–83.
Oettl L-L, Scheller M, Filosa C, Wieland S, Haag F, Loeb C, Durstewitz D, Shusterman R, Russo E, Kelsch W (2020) Phasic dopamine reinforces distinct striatal stimulus encoding in the olfactory tubercle driving dopaminergic reward prediction. Nat Commun 11:3460.
Paxinos G, Franklin K (2000) The Mouse Brain in Stereotaxic Coordinates, 2nd ed. San Diego: Academic Press.
Phillips PEM, Stuber GD, Heien MLA V, Wightman RM, Carelli RM (2003) Subsecond dopamine release promotes cocaine seeking. Nature 422:614–618.
Ramirez J-M, Baertsch NA (2018) The Dynamic Basis of Respiratory Rhythm Generation: One Breath at a Time. Annu Rev Neurosci 41:475–499.
Regan M (2018) K-Nearest-Neighbors-with-Dynamic-Time-Warping. Available at: https://github.com/markdregan/K-Nearest-Neighbors-with-Dynamic-Time-Warping.
Sakoe H, Chiba S (1978) Dynamic programming algorithm optimization for spoken word recognition. IEEE Trans Acoust 26:43–49.
Savitt JM, Jang SS, Mu W, Dawson VL, Dawson TM (2005) Bcl-x Is Required for Proper Development of the Mouse Substantia Nigra. The Journal of Neuroscience 25:6721–6728.
Scofield MD, Heinsbroek JA, Gipson CD, Kupchik YM, Spencer S, Smith ACW, Roberts-Wolfe D, Kalivas PW (2016) The Nucleus Accumbens: Mechanisms of Addiction across Drug Classes Reflect the Importance of Glutamate Homeostasis. Pharmacol Rev 68:816–871.
Shusterman R, Smear MC, Koulakov AA, Rinberg D (2011) Precise olfactory responses tile the sniff cycle. Nat Neurosci 14:1039–1044 Available at: http://dx.doi.org/10.1038/nn.2877.
Steen JB, Mohus I, Kvesetberg TK, Walloe L (1996) Olfaction in bird dogs during hunting. Acta Physiol Scand 157:115–119.
Stuber GD, Hnasko TS, Britt JP, Edwards RH, Bonci A (2010) Dopaminergic Terminals in the Nucleus Accumbens But Not the Dorsal Striatum Corelease Glutamate. Journal of Neuroscience.
Sugita T, Kanamaru M, Iizuka M, Sato K, Tsukada S, Kawamura M, Homma I, Izumizaki M (2015) Breathing is affected by dopamine D2-like receptors in the basolateral amygdala. Respir Physiol Neurobiol 209:23–27.
Sulzer D, Joyce MP, Lin L, Geldwert D, Haber SN, Hattori T, Rayport S (1998) Dopamine Neurons Make Glutamatergic Synapses in vitro. The Journal of Neuroscience 18:4588 LP – 4602.
Sun F et al. (2018) A Genetically Encoded Fluorescent Sensor Enables Rapid and Specific Detection of Dopamine in Flies, Fish, and Mice. Cell 174:481-496.e19.
Tong Q, Ye C, McCrimmon RJ, Dhillon H, Choi B, Kramer MD, Yu J, Yang Z, Christiansen LM, Lee CE, Choi CS, Zigman JM, Shulman GI, Sherwin RS, Elmquist JK, Lowell BB (2007) Synaptic Glutamate Release by Ventromedial Hypothalamic Neurons Is Part of the Neurocircuitry that Prevents Hypoglycemia. Cell Metab 5:383–393.
Uchida N, Kepecs A, Mainen ZF (2006) Seeing at a glance, smelling in a whiff: rapid forms of perceptual decision making. Nat Rev Neurosci 7:485–491.
Vann NC, Pham FD, Dorst KE, Del Negro CA (2018) Dbx1 Pre-Bötzinger Complex Interneurons Comprise the Core Inspiratory Oscillator for Breathing in Unanesthetized Adult Mice. eNeuro 5:ENEURO.0130-18.2018.
Wachowiak M (2011) All in a Sniff: Olfaction as a Model for Active Sensing. Neuron 71:962–973 Available at: http://linkinghub.elsevier.com/retrieve/pii/S0896627311007859.
Watabe-Uchida M, Zhu L, Ogawa SK, Vamanrao A, Uchida N (2012) Whole-Brain Mapping of Direct Inputs to Midbrain Dopamine Neurons. Neuron 74:858–873.
Welker WI (1964) Analysis of sniffing in the albino rat. Behavior 22:223–244.
Wesson DW (2020) The Tubular Striatum. Journal of Neuroscience 40:7379–7386.
Wesson DW, Donahou TN, Johnson MO, Wachowiak M (2008) Sniffing behavior of mice during performance in odor-guided tasks. Chem Senses 33:581–596 Available at:

http://www.ncbi.nlm.nih.gov/entrez/query.fcgi?cmd=Retrieve&db=PubMed&dopt=Citation&list_uids=18534995.
Wieland S, Schindler S, Huber C, Köhr G, Oswald MJ, Kelsch W (2015) Phasic Dopamine Modifies Sensory-Driven Output of Striatal Neurons through Synaptic Plasticity. The Journal of Neuroscience 35:9946–9956 Available at: http://www.jneurosci.org/content/35/27/9946.abstract.
Wise RA (2004) Dopamine, learning and motivation. Nat Rev Neurosci 5:483–494.
Yang H, de Jong JW, Tak Y, Peck J, Bateup HS, Lammel S (2018) Nucleus Accumbens Subnuclei Regulate Motivated Behavior via Direct Inhibition and Disinhibition of VTA Dopamine Subpopulations. Neuron 97:434-449.e4.
Youngentob SL, Mozell MM, Sheehe PR, Hornung DE (1987) A quantitative analysis of sniffing strategies in rats performing odor discrimination tasks. Physiol Behav 41:59–69.
Zahm DS, Heimer L (1987) The ventral striatopallidothalamic projection. III. Striatal cells of the olfactory tubercle establish direct synaptic contact with ventral pallidal cells projecting to mediodorsal thalamus. Brain Res 404:327–331.
Zhang Y-F et al. (2021) Ventral striatal islands of Calleja neurons control grooming in mice. Nat Neurosci 24:1699–1710.
Zhang Z, Liu Q, Wen P, Zhang J, Rao X, Zhou Z, Zhang H, He X, Li J, Zhou Z, Xu X, Zhang X, Luo R, Lv G, Li H, Cao P, Wang L, Xu F (2017) Activation of the dopaminergic pathway from VTA to the medial olfactory tubercle generates odor-preference and reward. Elife 6:e25423.
Zhao Y, Kerscher N, Eysel U, Funke K (2002) D1 and D2 receptor-mediated dopaminergic modulation of visual responses in cat dorsal lateral geniculate nucleus. J Physiol 539:223–238.

Acknowledgements:

We thank Jacqueline Sipio for help with histology and Ellyse Thomas for expert animal care assistance.

This work was supported by R01DC014443 and R01DC016519 to D.W.W., R01DA049545, R01DA049449 and R01NS117061 to D.W.W. and M.M., R01DC006213 to M.M., and R00HL159232 to A.G.V.. N.L.J. was supported by NIDCD T32015994 and F31DC020364.

848 **Figure Legends**
849
850 **Figure 1. Organization of midbrain dopamine input into the tubular striatum and nucleus**
851 **accumbens. A.** Schematic of anterograde tracing paradigm. DAT-IRES-Cre mice were injected
852 into their VTA with AAV.FLEX.hSyn.mGFP.synaptophysin.mRuby allowing for mGFP
853 expression in DAT+ cell bodies and synaptophysin.mRuby+ puncta in the terminals of DAT+
854 cells. Approximately 3 weeks later, coronal sections throughout the ventral striatum were collected
855 for later fluorescence imaging and quantification of synaptophysin.mRuby+ puncta. **B.** Example
856 of synaptophysin.mRuby expression throughout the ventral striatum, with key regions of interest
857 outlined by dashed lines. **C.** Quantification of synaptophysin+ puncta throughout the anterior-
858 posterior spans of regions of interest (*n*=6 mice). Data [puncta #'s/mm^2] are represented as mean
859 ± SEM. Data smoothed for visualization purposes only. **D.** Histograms representing data in (**C**)
860 with regions of interest segregated into their most anterior and posterior aspects (anterior most half
861 vs posterior most half). Data are mean ± SEM, points = individual mice. *p<0.5. abbreviations:
862 VTA (ventral tegmental area), NAcSh (nucleus accumbens shell), NAcC (nucleus accumbens
863 core), mTuS (medial aspect of the tubular striatum), LatTuS (lateral aspect of the tubular striatum),
864 PCX (piriform cortex). (the anterior or posterior-most 200µm were used for quantification of these
865 regions).
866
867 **Figure 2. Self-motivated spontaneous sniffing is associated with DA levels. A.** Diagram of the
868 setup for simultaneous measurement of respiration by means of both whole-body plethysmography
869 and an intranasal pressure cannula. One mouse was implanted with a cannula in its dorsal nasal
870 recess and placed in the plethysmograph. Intranasal pressure changes were monitored by a pressure
871 sensor connected to the cannula by a flexible tube passed through a fitted plug at the top of the
872 plethysmograph and compared to whole-body changes. Image made with BioRender. **Bi**. Overlaid
873 representative respiratory traces acquired from the plethysmograph (black) and intranasal cannula
874 (blue) from an awake mouse. Example of high frequency sniffing is shown zoomed in and the
875 expanded inset shows fidelity between the whole-body pressure and intranasal pressure signal. **Bii.**
876 Example of the latency difference between respiratory peaks recorded by intranasal pressure and
877 plethysmograph pressure during a high frequency sniffing bout with detected respiratory events
878 (*n*=125 respiratory cycles). Overlaid respiratory traces (top) shows an intranasal pressure peaks
879 aligned to time 0, and a pleth pressure peak detected <60ms later. The difference between peaks
880 was calculated and averaged across all 916 events; the whole-body plethysmograph trailed the
881 intranasal signal 0.028 ± 0.00s. **Biii**. Probability density histograms comparing respiratory
882 frequencies measured from the pleth and intranasal cannula. The plethysmograph reliably detected
883 sniffing at both low and high respiratory frequencies with >99% accuracy (916/919 respiratory
884 events). **C.** Schematic of fiber photometry and plethysmograph system used to simultaneously
885 record $GRAB_{DA}$ signals and sniffing behavior in unrestrained mice. Animals were injected with
886 AAV.hSyn-GRAB_DA1h and implanted with an optic fiber in the TuS, NAcSh, or NAcC. 3-5
887 weeks later, animals were placed in the plethysmograph and 465nm and 405nm light were passed
888 through dichroic mirrors before reaching the animal via patch cable and implanted optical fiber.
889 $GRAB_{DA}$ and UV emissions were amplified by photoreceivers before being digitized along with
890 simultaneous respiratory data. Image made with BioRender. **D.** Optic fiber implant locations in
891 the TuS, NAcSh, and NAcC (*n*=7 mice/group. Within each region, ellipse color corresponds to
892 same colored data in **Figures 2F-H and 3C-H**. **E.** Example of raw 465nm $GRAB_{DA}$ (green) and
893 405nm UV (purple) signals recorded in the TuS during a spontaneous sniff bout. Raw respiratory

trace (resp) is shown below with interpolated instantaneous frequency above (Inst Hz- black trace). Sniff duration is indicated by the grey shaded box. **Fi.** Averaged z-scored ΔF/F traces show an increase in $GRAB_{DA}$ levels in TuS during spontaneous sniff bouts. Average bout duration indicated by overlaid box plot. **Fii**. Significant positive correlation between $GRAB_{DA}$ levels in the TuS (the peak z-score during a spontaneous sniff bout) and sniffing vigor (average sniff frequency during bout) p=0.008. **Gi**. Averaged z-scored ΔF/F traces similarly show an increase in $GRAB_{DA}$ levels in the NAcSh during spontaneous sniff bouts. Average bout duration indicated by overlaid box plot. **Gii**. There was no correlation between $GRAB_{DA}$ levels in the NAcSh during spontaneous bout and sniffing vigor. **Hi**. Conversely, averaged z-scored ΔF/F traces show a decrease in $GRAB_{DA}$ levels in the NAcC during spontaneous sniff bouts. Average bout duration indicated by overlaid box plot. **Hii**. There was no significant correlation between $GRAB_{DA}$ levels in the NAcC during spontaneous bout and sniffing vigor (p>0.05). Abbreviations: resp (respiratory trace), Inst Hz (instantaneous frequency). Data in (Fi), (Gi), and (Hi) smoothed for visualization purposes only.

Figure 3. Bidirectional dopamine dynamics upon sensory-driven sniffing. A. Schematic of fiber photometry and plethysmograph system used to simultaneously record $GRAB_{DA}$ signals in the TuS, NAcSh, and NAcC and sniffing behavior in unrestrained mice (n=7/group) as used in Fig 2. Additionally, an olfactometer was used to deliver odors to animals in the plethysmograph, and a vibration motor (buzz) was attached to the outside of the plethysmograph. Image made with BioRender. **B.** Example of raw 465nm $GRAB_{DA}$ (green) and 405nm UV (purple) signals recorded in the TuS during an odor-evoked bout. Raw respiratory trace (resp) is shown below with interpolated instantaneous frequency above (Inst Hz- black trace). Grey shaded box denotes odor analysis window, starting 3 seconds following odor onset to account for the delay of odor delivery to the plethysmograph. **C-E.** Odor-evoked sniffing behavior and $GRAB_{DA}$ signals from mice with injections and optic ferrule implants in the TuS (C), NACSh (D), and NAcC (E). Average instantaneous sniffing frequency of TuS (Ci), NAcSh (Di), and NAcC (Ei) implanted mice across repeated odor presentations. Mean shown in black with individual mouse data across trials shown in light grey. Averaged z-scored ΔF/F across all 5 odor presentations in the TuS (Cii), NAcSh (Dii), and NAcC (Eii). Averaged peak of the z-scored $GRAB_{DA}$ response across trials in the TuS (Ciii), NAcSh (Diii), and NAcC (Eiii). Mean shown in black with individual mouse data across trials color coded to ellipse colors shown in **Figure 2D**. Significant positive correlations between $GRAB_{DA}$ levels (peak z-score during odor-evoked activity) and sniffing vigor (average sniff frequency during bout) in the TuS, (p<0.001, Civ) and NAcSh (p=0.002, Div) but not in the NAcC (Eiv). **F-H.** Buzz-evoked sniffing behavior and $GRAB_{DA}$ signals from same mice with injections and implants in the TuS (F), NAcSh (G), and NAcC (H). Average instantaneous sniffing frequency of TuS (Fi), NAcSh (Gi), and NAcC (Hi) implanted mice across repeated odor presentations. Mean shown in black with individual mouse data across trials shown in light grey. Averaged z-scored ΔF/F across all 5 odor presentations in the TuS (Fii), NAcSh (Gii), and NAcC (Hii). Horizontal line depicts 2s buzz duration. Averaged peak of the z-scored $GRAB_{DA}$ response across trials in the TuS (Fiii), NAcSh (Giii), and NAcC (Hiii). Mean shown in black with individual mouse data across trials color coded to ellipse colors shown in **Figure 2D**. Significant positive correlation between $GRAB_{DA}$ levels and sniffing vigor in the TuS, (p=0.01, Fiv), but not the NAcSh (Giv) or NAcC (Hiv). **I.** Comparison of the peak-evoked $GRAB_{DA}$ responses across the TuS, NAcSh, and NAcC during odor-, buzz-, and spontaneously-evoked sniffing. Data are represented as mean ±

SEM. Points = individual mice. ****p<0.0001, **p<0.01. Data shown in (Cii), (Dii), (Eii), (Fii), (Gii), and (Hii) are smoothed for visualization purposes only.

Figure 4. Initiation of sniffing by dopamine release into the ventral striatum. A. Schematic of optogenetically-evoked sniffing paradigm. DAT-IRES-Cre x Ai9 mice were injected with AAV-EF1α-DIO-hChR2(E123T/T159C)-EYFP in the VTA, and optic fibers terminating in the TuS, NAcSh or NAcC were implanted in the same surgery. Control mice were injected with AAV-Ef1α-DIO-EYFP. At least 4 weeks later, mice were tethered and placed in the plethsymograph to optogenetically stimulate DA terminal release while monitoring sniffing. Image (right) made with BioRender. **B.** Optic fiber implant locations in the TuS, NAcSh, and NAcC (n=6-11 mice/group). **C.** Example respiratory data from a TuS implanted mouse across 10 trials of light stimulation. Timing of the 1s long, 25Hz photostimulation depicted by grey shaded box and dotted blue horizontal line. Raw respiratory traces are shown on the left, and corresponding instantaneous frequency for each trial shown in the imagesc plots on the right. Dotted white line in image sc plots depicts stimulation onset. **D**. Imagesc plots across all mice tested within each group, showing individual trial data within mice. Example data from (C) denoted by the white star. Separation between mice marked by dark blue line. Stimulation onset is denoted by the vertical dotted white line, and 1s, 25Hz stimulation shown by the dotted blue trace. **E.** Mean sniffing frequency ± SEM during photostimulation across 10 trials in each group. **F.** Averaged z-scored respiratory frequency ± SEM of photostimulation-evoked sniffing. Stimulation onset denoted by vertical dotted black line and 25Hz, 1s duration by horizontal blue line. Group color legend matches what is shown in (E). **G**. Parameters of optogenetically-evoked sniffing during 1s photostimulation. All data presented as mean ± SEM, points = individual mice. ****p<0.0001, ***p<0.001, **p<0.01. **Gi.** Mean latency to sniff across groups. **Gii**. Mean percentage of time spent sniffing across groups. **Giii.** Mean sniffing vigor (max sniffing frequency reached during photostimulation). **Giv**. Mean probability that photostimulation will evoke sniffing. **H.** Averaged z-scored respiratory frequency during different photostimulation durations (100ms, 1s, 2s, 4s) compared to responses of EYFP controls stimulated for 1s in the TuS (Hi), NAcSh (Hii), and NAcC (Hiii). Insets in each panel show the percentage of time across all groups, calculated in a 4s window, that mice spend sniffing upon photostimulation.

Figure 5. State-dependence of a unique dopamine-evoked sniffing pattern. A. Example respiratory behavior of a TuS implanted mouse under urethane anesthesia. Raw respiratory traces (left) and corresponding imagesc plots (right) across 10 trials of photostimulation. 1s long, 25Hz photostimulation duration depicted by grey shaded box and dotted blue horizontal line. Dotted white line in the imagesc plot = photostimulation onset **B.** Imagesc plots across 5 representative mice per group showing individual trial data within mice. Starred data represents example data from (A). Separation between mice denoted by dark blue line. Stimulation onset is denoted by the vertical dotted white line, and 1s, 25Hz stimulation shown by the dotted blue trace. **C.** Averaged z-scored respiratory frequency of photostimulation-evoked sniffing. Stimulation onset denoted by vertical dotted black line and duration by horizontal blue dotted line. Inset shows the evoked z-scored average across all groups during light stimulation. **D.** Overview of machine learning applied to respiratory traces starting with dynamic time warping (DTW) between a 1s odor-evoked sniff bout and 1s opto-evoked sniff bout. Bin size=10ms. 1s-long respiratory traces (100Hz) were converted to instantaneous frequency traces (also 1s long) and subjected to DTW to assess distance in proximal time-points. Subsequently, a model was trained on experimenter-identified traces from

either buzz-, odor-, spontaneous-, or photostimulation-evoked respiration that were also previously subjected to DTW (see Methods). **E.** Confusion matrix displaying the classifier accuracy in predicting optogenetic-, odor-, buzz-, or spontaneously-evoked sniffing bouts. Classifier was trained on 80% of samples and tested on remaining 20%.

Figure 6. Sniffing recruits the activity of D1 and D2 spiny projection neurons. A. Schematic of the fiber photometry system for use in head-fixed mice. D1- or D2- cre mice were injected with AAV.hSyn.Flex.GCaMP6f.WPRE.SV40, and implanted with an optical fiber terminating in the TuS. Mice also received a headbar for later fixation. Odors were delivered directly to the animal's nose, and respiration was recorded with an extranasal flow sensor. Image made with BioRender. **B.** Optic fiber implant locations in the TuS across D1- and D2-cre mice. **C.** GCaMP activity of D1 and D2 neurons in the TuS during spontaneously-evoked sniffing. **Ci.** Averaged z-scored ΔF/F of D1 and D2 neurons aligned to spontaneous sniff bout onset (D1, n=4, 2 points/mouse. D2, n=5, 2points/mouse. Overlaid box plots represent average bout duration. **Cii.** Average peak of GCaMP evoked z-scored activity during spontaneous sniffing. **Ciii.** Mean sniffing instantaneous frequency during spontaneous bouts. **Civ.** There was no correlation between GCaMP levels in D1 neurons (peak z-score during a bout) during spontaneous sniffing and sniffing vigor (average sniff frequency during the bout; p>0.05). **Cv.** There was a significant positive correlation between GCaMP levels in D2 neurons during spontaneous bouts and sniffing vigor (p<0.0001). **D.** GCaMP activity of D1 and D2 neurons in the TuS during odor-evoked sniffing. **Di.** Average instantaneous sniffing frequency of both D1-cre (n=1, 2 sessions/mouse) and D2-cre (n=5, 2 sessions/mouse) mice across repeated odor presentations, with individual mouse data across trials shown in light grey. **Dii.** Averaged z-scored ΔF/F across 4 odor presentations in D1-mice. Odor duration depicted by horizontal line. **Diii.** Averaged peak of the z-scored GCaMP response in D1-cre mice across trials. **Div.** Averaged z-scored ΔF/F across 4 odor presentations in D2-mice. Odor duration depicted by horizontal line. **Dv**. Averaged peak of the z-scored GCaMP response in D2-cre mice across trials. **Dvi.** Overlayed averages of peak z-score GCaMP responses from D1- and D2-cre mice across trials. Data in (Ci),(Dii) and (Div) smoothed for visualization purposes only.

Figure 7. Dopamine binding to D1 and D2 ventral striatum receptors contributes to sniffing. A. Bilateral cannulae implant locations in the TuS and NAcSh. Colored for visualization purposes only. Position relative to bregma. B. Diagram of pharmacological manipulation and behavioral paradigm. Animals were implanted with stainless steel, bilateral cannulae with tips terminating in the TuS (n=13) or NAcSh (n=13). After surgical recovery, animals underwent behavioral testing. In a counterbalanced, within-subjects design, animals were administered an intracranial infusion of a selective D1, D2, or D3 antagonist or corresponding vehicle control 10min prior to being placed in the plethysmograph. Vehicle = sterile saline + 0-12% DMSO. During a behavioral session, animals were presented with both olfactory and non-olfactory (buzz) stimuli. Image made with BioRender. **C.** Impact of selective antagonism of D1- (Ci), D2- (Cii), and D3-receptors (Ciii) on spontaneous sniffing. D3 antagonism had no effect on spontaneous sniffing in the TuS or NAcSh (Ciii, p>0.05). **D.** Impact of selective antagonism of D1- (Di), D2- (Dii), and D3-receptors (Diii) on odor-evoked sniffing. D1 and D3 antagonism had no effect on odor-evoked sniffing in the TuS or NAc (Di & Diii, p>0.05). **E.** Impact of selective antagonism of D1- (Ei), D2- (Eii), and D3-receptors (Eiii) on buzz-evoked sniffing. D2 and D3 antagonism had no effect on buzz-evoked sniffing in the TuS or NAc (Eii & Eiii, p>0.05). Data are mean (dark bolded line) ± SEM, lighter

lines = individual mice. Abbreviations: SCH (D1 antagonist SCH23390), RAC (D2 antagonist raclopride), PG0 (D3 antagonist PG010370), VEH (vehicle). ****$p<0.0001$, **$p<0.01$, *$p<0.05$.

Methods

Animals

Male and female mice were housed on a 12:12hr light-dark cycle with *ad libitum* access to food and water. All behavioral testing took place during the light cycle. Mice with viral injections alone were group housed (≤5 mice/cage) and any mouse with a chronic implant was single housed following its surgical procedure. Food (Envigo Teklad Global, 18% rodent diet irradiated pellet, Cat # 2018; Indianapolis, IN) and reverse osmosis water were available *ad libitum* except during behavioral monitoring/recordings. Mice were housed in standard shoebox sized plastic cages (Allentown Jag 75 micro-vent system; Allentown, PA; L: 29.2cm W: 18.5cm H:12.7cm) on a rack made for individually vented cages. Corncob bedding and a Nestlet™ (Ancare; Bellmore, NY) were in each cage along with manzanita sticks (Bio-Serve). Mice were housed on a 600-1800hr light cycle with lights on during the daytime. Temperature in the room averaged 70 ± 2˚F, with 30-70% humidity and 10-15 room air changes per hour. The housing room was specific pathogen free. Observation occurred from 1000-1700hrs. All animal care was conducted with in the AAALAC animal research program of the University of Florida, in accordance with the guidelines from the Guide for the Care and Use of Laboratory Animals and approved by the University of Florida Institutional Animal Care and Use Committee.

Mouse lines included the following transgenic lines which all were maintained on a C57BL/6J background (Jackson labs, strain #000664; RRID:IMSR_JAX:000664) and were bred in house within a University of Florida vivarium. *drd1-Cre* and *drd-2-Cre* lines (Gong et al., 2007) were obtained from the UC Davis Mutant Mouse Regional Resource Center (D1: EY262Gsat/Mmucd; D2: ER44Gsat). DAT^{IRES}-Cre mice (Bäckman et al., 2006; strain #006660; RRID: IMSR_JAX:006660), TH-Cre mice (Savitt et al., 2005); strain #008601; RRID: IMSR_JAX:008601), VGluT2 fl/fl mice (Tong et al., 2007); strain #012898; RRID: IMSR_JAX:012898), and Ai9 TdTomato Cre reporter mice (Madisen et al., 2010; strain # 007909, IMSR_JAX:007909) were obtained from Jackson labs. A total of 145 mice (mixed sexes) were used in this study for experimentation. Out of these, a total number of 41 were excluded form data analyses due to experimental issues (*e.g.,* surgical complications, off-target brain implants, viral injections which missed the target).

For all surgical procedures, under aseptic conditions, mice were anesthetized with Isoflurane (2-4% in oxygen, IsoFlo®, Patterson Veterinary) and mounted in a stereotaxic frame where they were maintained under Isoflurane. Body temperatures were maintained with a 38ºC heating pad underneath. A local anesthetic, bupivacaine hydrochloride (Marcaine™, 5mg/kg subcutaneously, s.c., Patterson Veterinary), and the analgesic meloxicam (5mg/kg, s.c., Patterson Veterinary) were administered before incision and exposure of the skull. Mice receiving chronic implants (*e.g.,* cannulae, optic fibers) were given meloxicam (0.5mg/kg, s.c.) for 3 days following surgery.

For viral injections, craniotomies were made over the ventral tegmental area (VTA) (-3.6AP/0.35ML/-4.75DV), tubular striatum (TuS) (1.4AP/1ML/-4.90DV), nucleus accumbens shell (NAcSh) (1.4AP/1ML/-4.40DV), and/or nucleus accumbens core (NAcC),(1.4AP/1ML/-3.90DV) and a pulled glass micropipette containing the AAV was lowered into the region of interest. Viruses were all delivered via the pulled pipette attached to a Nanoject III (Drummond Scientific) at a rate of 2nl/s unless otherwise noted. After waiting 10min, the pipette was slowly

withdrawn from the brain. Unless followed by an implant in the same surgery, craniotomies were sealed with dental wax, and the incision closed with wound clips.

For intranasal 'sniff' cannula implantation, a ~1mm diameter hole was drilled through the right nasal bone, 1.5mm anterior the frontal/nasal fissure and 0.5mm lateral following prior methods (Wesson et al., 2008). A stainless-steel guide cannula (22GA, #C313G, P1 Technologies, Roanoke, VA) cut to extend 0.5mm below the pedestal was lowered through the craniotomy and secured with dental cement. A dummy cannula (#C313DC, P1 Technologies, Roanoke, VA) cut to extend 0.2mm past the guide cannula was also inserted when not recording from the mouse.

To record respiration, the dummy cannula was removed and a pressure transducer was connected (CPXL04GF, Honeywell) to the cannula via a piece flexible piece of polyethylene tubing. The mouse was then placed in the plethysmograph and recorded for 15min. Plethysmograph-recorded transients were detected using a flow transducer (Data Sciences International) and digitized at 300Hz (0.1-12Hz band pass; Tucker Davis Technologies, Alachua, FL), following a 500x gain amplification (Cyngus Technology Inc, Southport, NC). Intranasal pressure transients were amplified and digitized using the same settings.

Anatomical Tracing

For synaptophysin injections, a craniotomy was made over the VTA, and a micropipette containing 100nL of pAAV-hSyn-FLEx-mGFP-2A-Synaptophysin-mRuby (Addgene 71760-AAV1; titer: 9.8×10^{12}vg/mL) was injected unilaterally into the VTA of DAT-IRES-Cre mice.

3 weeks following injections, mice were overdosed with sodium pentobarbital (Fatal-Plus, Patterson Veterinary) and transcardially perfused with 0.9% saline followed by 10% phosphate-buffered formalin. Brains were removed and stored in a 10% formalin in 30% sucrose solution at 4ºC prior to sectioning. Brains were coronally sectioned at 40µm and sections were stored in Tris-buffered saline with 0.03% sodium azide.

Image acquisition and quantification

Brain regions of interest were identified using the mouse brain atlas (Paxinos and Franklin, 2000). For the TuS, 12 images were acquired spanning 1.94mm - 0.14mm anterior to Bregma. For the nucleus accumbens, a total of 8 images were acquired spanning 1.94mm – 0.74mm anterior Bregma.

Images were acquired with a Nikon Eclipse Ti2e fluorescent microscope. For brains with synaptophysin injections (n=6 mice), images were acquired at 20x magnification across the hemisphere ipsilateral to the injection site, and Z-stacked at every 4µm. For quantification, regions of interest (ROIs) were drawn around areas of interest, namely the NAcC and NAcSh along with the medial and lateral TuS. To determine the medial and lateral portions, the TuS was divided into thirds and the most medial or lateral third was used to ensure distinctness between the two regions (Martin-Lopez et al., 2019). Images were preprocessed to decrease average background fluorescence and enhance contrast. A semiautomated counting algorithm created within NIS elements software (Nikon) was used to detect and count fluorescent puncta, allowing for an

unbiased estimation of puncta numbers. Puncta were identified and quantified based on their size and fluorescence intensity via bright-spot detection.

To reconstruct synaptophysin injection sites **(Fig S1)**, the VTA was imaged from -2.92 to -3.80mm posterior bregma, as identified with use of a brain atlas(Paxinos and Franklin, 2000). Next, an experimenter (A. C.-L.) identified and marked GFP+ cell bodies in VTA schematics within Adobe Illustrator.

Fiber photometric recording in the plethysmograph

Virus injection and optical fiber implant

WT mice were injected unilaterally in the NAcSh, NAcC, or TuS (*n*=7/group) with 100nL pAAV.hSyn-GRAB_DA1h (Addgene 113050, titer: $1x10^{13}$vg/mL). Viral injections were performed as previously described (see 'Animals'). In the same surgery, a 400µm core, 0.48NA optical fiber secured in a 2.5mm outer diameter metal ferrule was chronically implanted to terminate in the TuS, NAcSh, or NAcC and affixed to the skull with dental cement. Animals were recorded from 3-5 weeks following surgery.

Photometry

465nm ($GRAB_{DA}$ excitation wavelength, driven at 210Hz) and 405nm (UV excitation wavelength, driven at 330Hz; control) light emitting diodes (TDT, RZ10x) were coupled to a fluorescent minicube (Doric lenses, FMC6) via 200µm, 0.22NA FCM optic fiber patch cords. Both excitation and emission light were directed through a single 400µm, 0.57NA patch cord connected to the animal by the implanted 2.5mm metal ferrule. Emission light was directed through the mini cube and coupled to femtowatt photoreceivers to monitor GFP and UV signals (TDT, RZ10x). The emission signals were low-pass filtered (6th order), pulse demodulated, and digitized (1kHz) using a Tucker Davis Technologies processor (TDT). All parameters for imaging and acquisition of photometry data were consistent across all groups.

Respiratory data acquisition

To simultaneously monitor photometry signals and respiration, mice were gently tethered to the patch cord and placed in a whole-body plethysmograph (Data Sciences International, St. Paul, MN). Respiratory transients were detected using a flow transducer (Data Sciences International) and digitized at 300Hz (0.1-12Hz band pass; Tucker Davis Technologies, Alachua, FL), following a 500x gain amplification (Cyngus Technology Inc, Southport, NC).

Behavioral monitoring

Behavioral sessions lasted approximately 30min during which mice were presented with both olfactory and non-olfactory stimuli. To allow for examination of spontaneous sniffing, we included 5min periods where no stimuli were presented at the beginning (0-5min), middle (12-17min), and end (28-33min) of a session. Between 5-12min, 2 trials of 4 different stimuli were pseudorandomly presented. The final 3 trials of pseudorandom stimuli presentations occurred between 17-28min. Each stimulus was presented for 2s with a 60s inter-trial interval.

Stimulus delivery

Odors R(+)-limonene and thioglycolic acid (Sigma-Aldrich, >97% purity), and that of peanut oil (La Tourangelle®, Woodland, CA), were presented to mice via a custom air-dilution odor delivery

1213 device connected to the plethysmograph. During experimentation, 2mL of all odors were contained
1214 in 40mL glass headspace vials at room temperature. Computer-controlled and user-initiated
1215 openings of valves allowed for odors to pass through headspace vials at a flow rate of 50mL/min,
1216 following which they were mixed with a carrier stream of clean filtered room air delivered by a
1217 pump (1L/min; Tetra Whisper, Melle, Germany) before being introduced into the plethysmograph.
1218 All odors were handled within independent tubing to prevent cross-contamination. Following each
1219 odor presentation, odor-vaporized air was passively cleared from the plethysmograph through an
1220 exhaust outlet at the chamber's ceiling since the filtered room air is continuously delivered.
1221 Serving as a non-olfactory stimulus, a vibration motor (3V, 12000 RPM; BestTong), referred to as
1222 "buzz," was secured to the outside of the plethysmograph. During trials of pseudorandom stimulus
1223 presentations, each stimulus was presented for 2s with a 60s inter-trial interval.
1224
1225 **Fiber photometric recording in head-fixed mice**
1226 *Virus injection and optical fiber implant*
1227 Mice for this method were also used for data collection and their results published (albeit from
1228 different stimulus conditions wherein analyses were performed on well-learned odor-associated
1229 pairs) in a prior study (Gadziola et al., 2020). As we previously described in that study, *D1-Cre*
1230 and *D2-Cre* mice were injected in the TuS with 1µL AAV5-EF1α-DIO-GCaMP6f-WPRE
1231 (obtained from the Penn Vector Core in the Gene Therapy Program of the University of
1232 Pennsylvania, 5.43×10^{13}GC/mL). Viral injections were performed as described above (see
1233 'Animals'). Two weeks later, a 400µm core, 0.48NA optical fiber secured in a 2.5mm metal ferrule
1234 was chronically implanted to terminate in the TuS. A plastic head-bar was also affixed to the skull
1235 with dental cement for later head fixation. Animals were given a week for surgical recovery before
1236 undergoing behavioral testing.
1237
1238 *Imaging*
1239 465nm (GCaMP excitation wavelength, driven at 210Hz) and 405nm (UV excitation wavelength,
1240 driven at 330Hz; control) light emitting diodes were coupled to a 5 port minicube (Doric lenses,
1241 FCM5) using 400µm, 0.48NA FCM optic fiber patch cords. Both excitation and emission light
1242 were directed through a patch cord connected to the animal by the implanted 2.5mm metal ferrule.
1243 Emission light was directed through the 5-port mini cube and coupled to femtowatt photoreceivers
1244 to monitor GFP and UV signals. The data were then digitized and pulse demodulated at 1kHz
1245 using a Tucker Davis Technologies processor (TDT). All parameters for imaging and acquisition
1246 of photometry data were consistent across D1- and D2-Cre mice.
1247
1248 *Behavioral sessions*
1249 Animals were head-fixed and presented with sets of 3 novel odors, 4 times each. To enhance each
1250 animal's contribution to a more rigorous data set, animals were tested a second time at least 24hrs
1251 later with sets of 3 different novel odors. Odors were delivered for 2s duration with a 17 ± 2s inter-
1252 trial interval through an odor port positioned 1cm from the animal's snout.
1253
1254 *Stimulus delivery*
1255 Odors were presented through an olfactometer and delivered through an odor port positioned 1cm
1256 from the animal's snout. Odors included ethyl butyrate, 1,7-octadiene, isopentyl acetate, heptanal,
1257 2-heptanone, R(+)-limonene, ethyl propionate, S(-)-limonene, methanol, methyl valerate, 2-
1258 butanone, 1,4-cineole, butanal, propyl acetate, allylbenzene, allyl bromide, isobutyl propionate,

and 2-methylbutyraldehyde (Sigma Aldrich, all > 97% purity). Odors were diluted to 1Torr in mineral oil and further diluted by mixing 100mL odor vaporized N_2 with 900mL medical grade N_2 (Airgas). Stimuli were therefore presented at a total flow rate of 1L/min. Odor was continuously flowing to the odor port but removed by a vacuum prior to reaching the animal. Odor sets used varied across animals and across sessions.

Respiratory data acquisition

Respiration was recorded via an extranasal flow sensor (CPXL04GF, Honeywell) positioned near the animal's nose as described (Jordan et al., 2018). A 1/8" inner diameter hose which terminated into the flow sensor was placed ~7-10mm from the nose of the mouse during head fixation.

Optogenetic stimulation of mice in the plethysmograph

Virus injection and fiber implant

DAT^{IRES}-Cre x Ai9 mice or VGluT2 fl/fl x TH-Cre mice were injected unilaterally in the VTA with 400nL AAV5-EF1α-DIO-hChR2(E123T/T159C)-EYFP (Addgene 35509, titer: $1.3x10^{13}$vg/mL) or AAV5-EF1α-DIO-EYFP (for controls, UNC vector Core, titer: $3.5x10^{12}$vg/mL). Viral injections were performed as previously described. In the same surgery, a 300µm core 0.39 NA optical fiber in a ceramic ferrule was chronically implanted to terminate in the TuS, NAcSh, or NAcC in DAT^{IRES}-Cre x Ai9 mice or in the TuS for VGluT2 fl/fl x TH-Cre and affixed to the skull with dental cement. Animals were tested no sooner than 4 weeks following surgery.

To reconstruct ChR2.EYFP injection sites in the VTA of DAT^{IRES}-CRE mice (**Fig S2**), the VTA was imaged from -2.92 to -3.80mm posterior bregma, as identified with use of a brain atlas (Paxinos and Franklin, 2000). An independent rater used illutrator to trace density of expression across images.

Light stimulation and behavioral monitoring

Optogenetic stimulation (25Hz, 15ms pulse width, 1s duration) was delivered by a 473nm laser (CrystaLaser, DL473-100). This paradigm was based on prior studies and pilot work done in the lab. A 300µm , 0.39NA fiber connected the laser to an optic rotary joint, and a 400µm , 0.47NA fiber connected the rotary joint to the mouse. Animals (DAT^{IRES}-Cre: TuS *n*=11, NAcSh *n*=6, NAcC *n*=6, EYFP controls *n*=9; VGluT2 fl/fl x TH-Cre: TuS *n*=4, EYFP controls *n*=4) received one habituation day wherein they were gently tethered to the path cable and placed in the plethysmograph for 20mins. The following day, animals were again tethered, placed in the plethysmograph, and given a brief, 5min habituation period. Following this, photostimulations (7-10/mouse) were delivered with a 2 ± 1min inter-trial interval.

A subset of DAT^{IRES}-Cre x Ai9 (TuS: *n*=5, NAcSh: *n*=4, NAcC: *n*=4, EYFP controls: *n*=6) underwent testing with varying durations of photostimulation. Stimulations at 25Hz with a 15ms pulse width were delivered for durations of 120ms, 1s, 2s, or 4s. After a habituation day, mice received a single stimulation parameter per day over four consecutive days. Each mouse underwent the 1s duration on day 1, and the following 3 stimulation paradigms were randomized across mice over the remaining 3 testing days. Photostimulations (9-11/mouse) were delivered with a 2 ± 1min inter-trial interval.

Concluding testing, the same mice were then deeply anesthetized with urethane (1g/kg i.p.; Sigma Life Science), tethered, and placed in the plethysmograph and photostimulated as above. Mice were transcardially perfused following recordings and within 30mins of urethane administration.

Machine learning to classify respiration

The study utilized a dataset comprising differently evoked sniffing data which consist of 261 samples, each 1s long. The dataset consisted of time series data representing respiratory frequencies (10ms bins).

Dynamic Time Warping (DTW) was employed as the distance metric for measuring the similarity between the time series data (respiratory frequency). DTW is known for its ability to align and compare time series data. DTW involves finding the optimal alignment between sets of data points of two sequences by warping the time axes. This allows the comparison of sequences with different lengths or different temporal structures. DTW creates a cost matrix, where each element represents the distance or dissimilarity between corresponding points in each of the two time series. Dynamic programming is used to efficiently find the optimal alignment by considering all possible alignments and selecting the one with the lowest cumulative distance (Sakoe and Chiba, 1978)

The k-Nearest Neighbors (k-NN) algorithm was utilized for classification of unknown data points based on the majority class of its k-nearest neighbors in the feature space. In the context of time series data, DTW can be used as a distance metric in the k-NN algorithm instead of using traditional Euclidean distance. For a given query time series, the algorithm identifies the k-NN from the training set based on DTW distance (Bagnall et al., 2017). For each query time series, the k-NN were identified and a majority voting scheme was employed to assign the class label.
Prior to applying the DTW k-NN algorithm, time series data were applied min-max normalization to ensure a uniform scale across all features. Subsequently, the dataset was divided into training and testing sets, with 80% of the samples allocated for training (208 samples) and 20% for testing (53 samples). The performance of the DTW k-NN algorithm was evaluated in terms of its accuracy, precision, recall, and F1-score. The max warping window was set at 7 and k at 3 which identified the combination that maximized the performance metrics during experiments.

The experiments were conducted using Google Colab (Google Brain Team, Mountain View, CA, USA). The DTW k-NN algorithm (Regan, 2018) was implemented in Python, utilizing the code available in the GitHub repository: https://github.com/markdregan/K-Nearest-Neighbors-with-Dynamic-Time-Warping. The dataset consisted of 63 photostimulation-evoked, 65 odor-evoked, 63 buzz-evoked, and 70 spontaneous respiratory/sniff bouts (N=261 total samples).

Pharmacological manipulations

Intracranial cannulae implantation

Bilateral craniotomies were made to target the the TuS and NAcSh. Stainless steel bilateral guide cannulae (26GA, 2.0mm center-to-center distance, 5.3mm long from the base of the pedestal, P1 Technologies, Roanoke, VA) were lowered either to target the TuS (n=13) or the NAcSh (n=13). Cannulae were affixed to the skull via dental cement, and dummy cannulae with a 0.5mm projection from the end of the guide cannulae were then inserted and dust caps were added.

Selective antagonists and intracranial infusions

SCH23390 (Tocris Bioscience, Bristol, UK) was dissolved in 0.9% sterile saline to a concentration of 0.5µg/µL. 0.1µL was infused to deliver 0.05µg/hemisphere. Raclopride (Tocris Bioscience, Bristol, UK) was dissolved in 0.9% saline + 5% dimethyl sulfoxide to a concentration of 23.8µg/µL, and 0.21µL was infused to deliver 5µg/hemisphere. PG01037 (Tocris Bioscience, Bristol, UK) was dissolved in 0.9% saline + 12% DMSO to a concentration of 20µg/µL. 0.15µL was infused to achieve 3µg/hemisphere. Internal cannulae that were cut at lengths projecting 0.5mm past the guide cannulae and thus terminating in the TuS or NAc were connected to 25GA polyurethane tubing (Instech Laboratories, Plymouth Meeting, PA) backfilled with dH2O. 1µL Hamilton syringes (Reno, NV) were used to inject total volumes ranging from 0.1-0.21µL. Mice were gently scruffed, dust caps and dummy cannulae were removed, and the internal cannulae was inserted before mice were placed back in their home cages for infusions. All drugs were infused at a rate of 0.1µL/min followed by a 2min rest period before the internal cannulae was removed, dummy cannulae and dustcap replaced. For all groups, behavioral testing began 10min following the start of drug infusion. All mice were tested across a 6 week period and recieved all selective antagonists and their corresponding vehicles, with 7 days between testing sessions.

Behavioral methods

To monitor spontaneous and sensory-evoked sniffing behavior, mice were placed in the plethysmograph and underwent behavioral testing and stimulus delivery as previously described to monitor odor-, buzz-, and spontaneously-evoked sniffing (see *Fiber photometry imaging of DA release in the ventral striatum.*)

Histology

Mice receiving synaptophysin injections were perfused 3 weeks following injection. Mice undergoing behavior were perfused following the last day of behavioral monitoring. All mice were overdosed with sodium pentobarbital (Fatal-Plus, Patterson Veterinary) and transcardially perfused with 0.9% saline followed by 10% phosphate-buffered formalin. Brains were removed and stored (at 4ºC) in a 10% formalin in 30% sucrose solution prior to sectioning. Brains were coronally sectioned at 40µm and sections were stored in Tris-buffered saline with 0.03% sodium azide. Microscopic examination of tissue occurred on a Ti2e inverted fluorescent microscope, and only mice with on-target manipulations (cannulae locations, viral injections, viral injections + optic fiber placements) contributed to data sets. Verification of brain regions and target sites was aided by use of a brain atlas (Paxinos and Franklin, 2000).

Quantification and Statistical Analysis

Analysis of respiratory data.

Inhalation peaks (sampled at 300Hz) were detected offline in Spike2 (Cambridge Electronic Design, Cambridge, UK). First, the respiratory data were filtered (0.1-12Hz band pass). Second, the maximum point of each respiratory cycle was identified, and instantaneous frequency was then calculated based off of the duration between one peak and its preceding peak. Data were down-sampled to 100Hz for subsequent analyses.

Analysis of fiber photometry data.

Offline using a custom script in Spike 2, the GFP and UV signals were filtered (2nd order, 25Hz low pass) and smoothed with a sliding window (9 bins averaged). A first-degree polynomial fit

was used to find the relationship between the signal and control channels and generate a scaled control channel. The fitted control channel was subtracted from the signal channel and z-scored ΔF/F traces were calculated using a 3s pre-event baseline window ($GRAB_{DA}$ analysis) or 2s pre-event baseline window (GCaMP6f for D1- and D2-Cre analysis).

Based on a series of pilot experiments, we found that on average, tethered animals in the plethysmograph typically do not perceive odors until 3s following odor control valve opening (as indicated by their reflexive/orienting sniffing responses). To account for this delay, the 3s after valve opening and odor onset serve as the pre-event baseline. Buzz-evoked $GRAB_{DA}$ signals were analyzed relative to the buzz onset, and spontaneous sniffing was analyzed relative to bout onset.

Peak $GRAB_{DA}$ signals and average sniff frequency were calculated within the 4s following odor analysis onset, 2s buzz duration, or spontaneous bout. Spontaneous sniffing bout durations varied and were identified based on prolonged periods of sniffing at frequencies ≥6Hz for ≥1s. Given the highly dynamic nature of sniffing and the rapid shift between respiratory frequencies in mice, we identified individual spontaneous sniff bouts wherein the mouse was sniffing at frequencies <6Hz for at least 2s prior to bout onset.

For D1- and D2-Cre GCaMP6f photometry, because animals were head-fixed and odor was delivered directly to the nose with high temporal precision, the 2s before odor delivery was used as the trial specific baseline for the z-scored ΔF/F values.

Additional statistical methods

Data were analyzed in GraphPad Prism. All performed statistical tests were two-sided. Sample sizes are consistent with those reported in the field. All data are reported as mean ± SEM unless otherwise reported. Specific tests and *p* values used can be found in the Results section or the figure legends.

Johnson et al., Figure 1

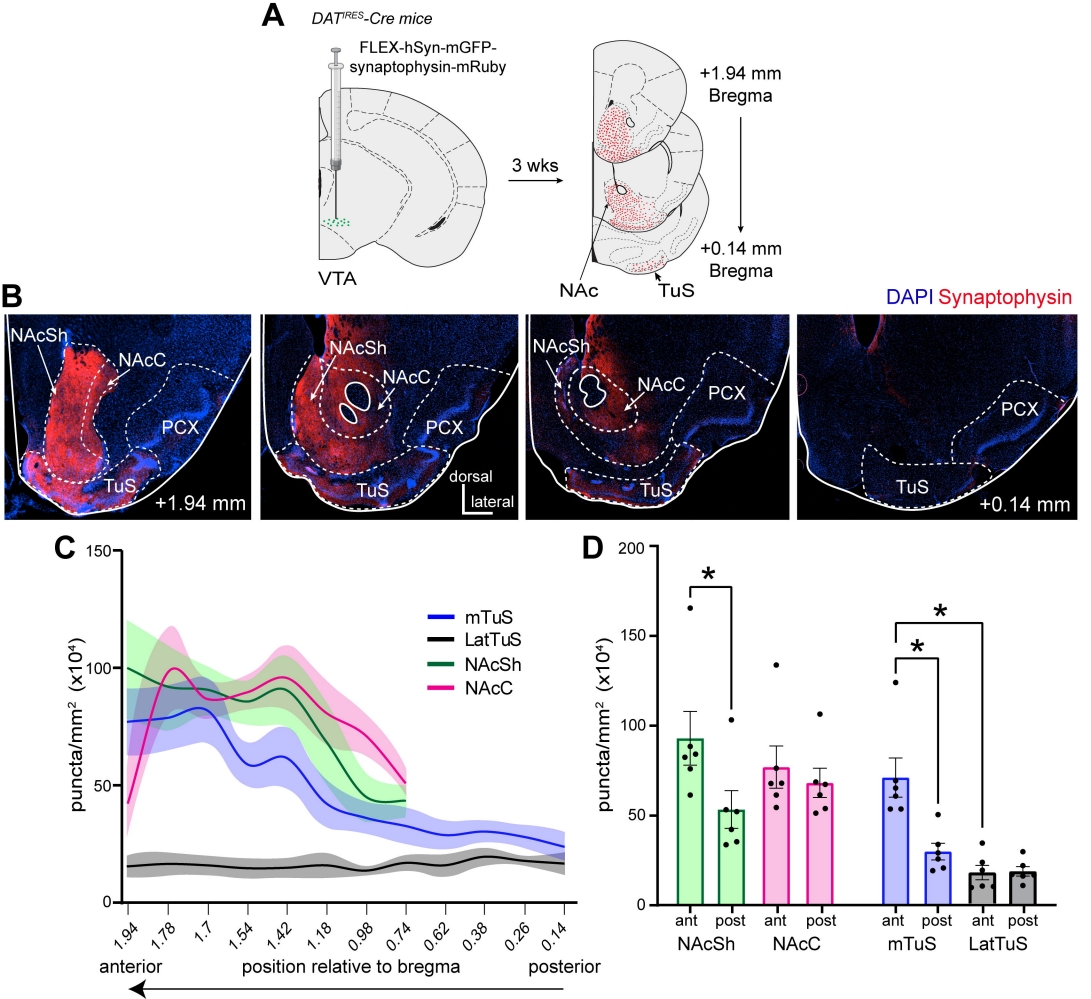

Johnson et al., Figure 2

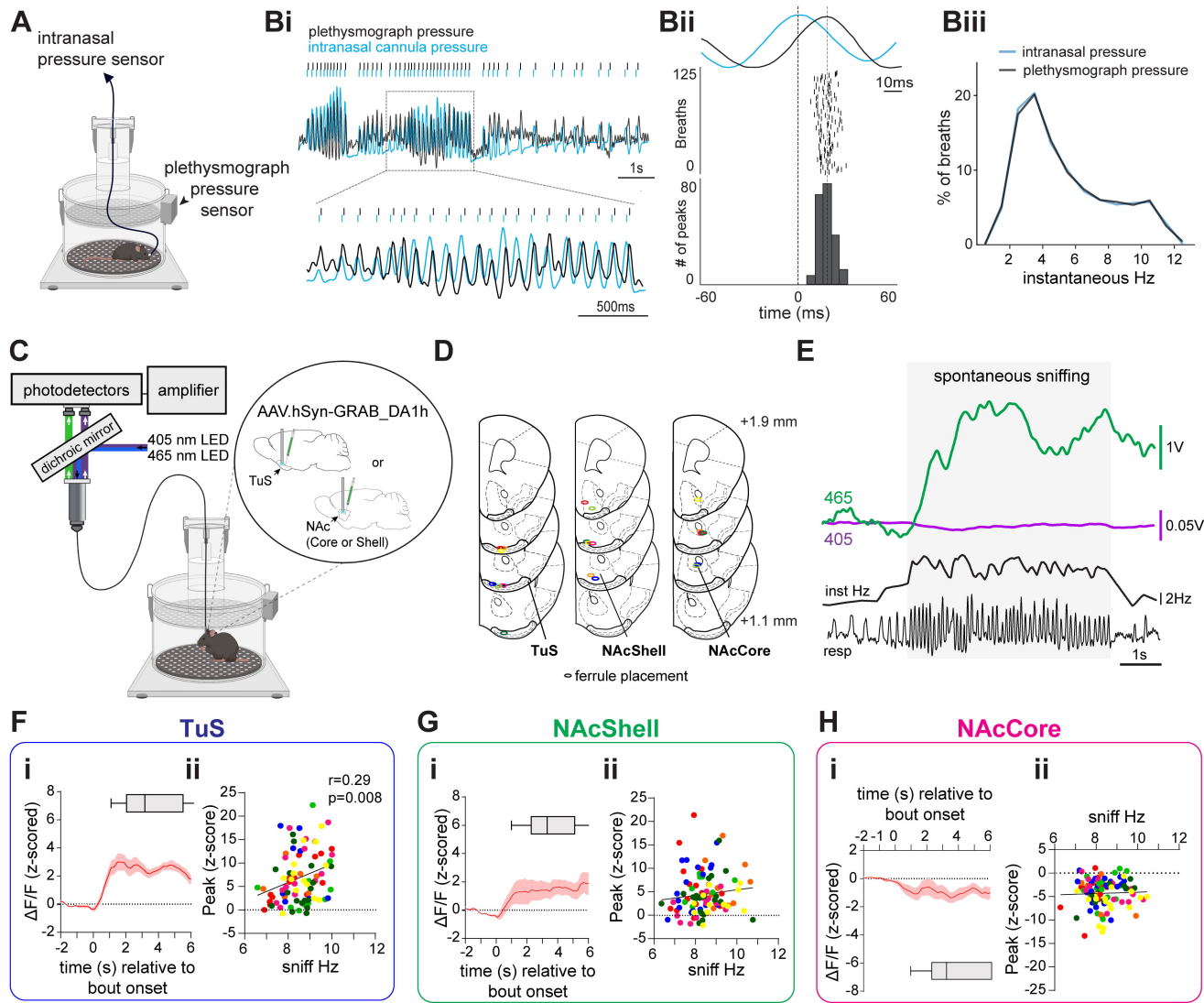

Johnson et al., Figure 3

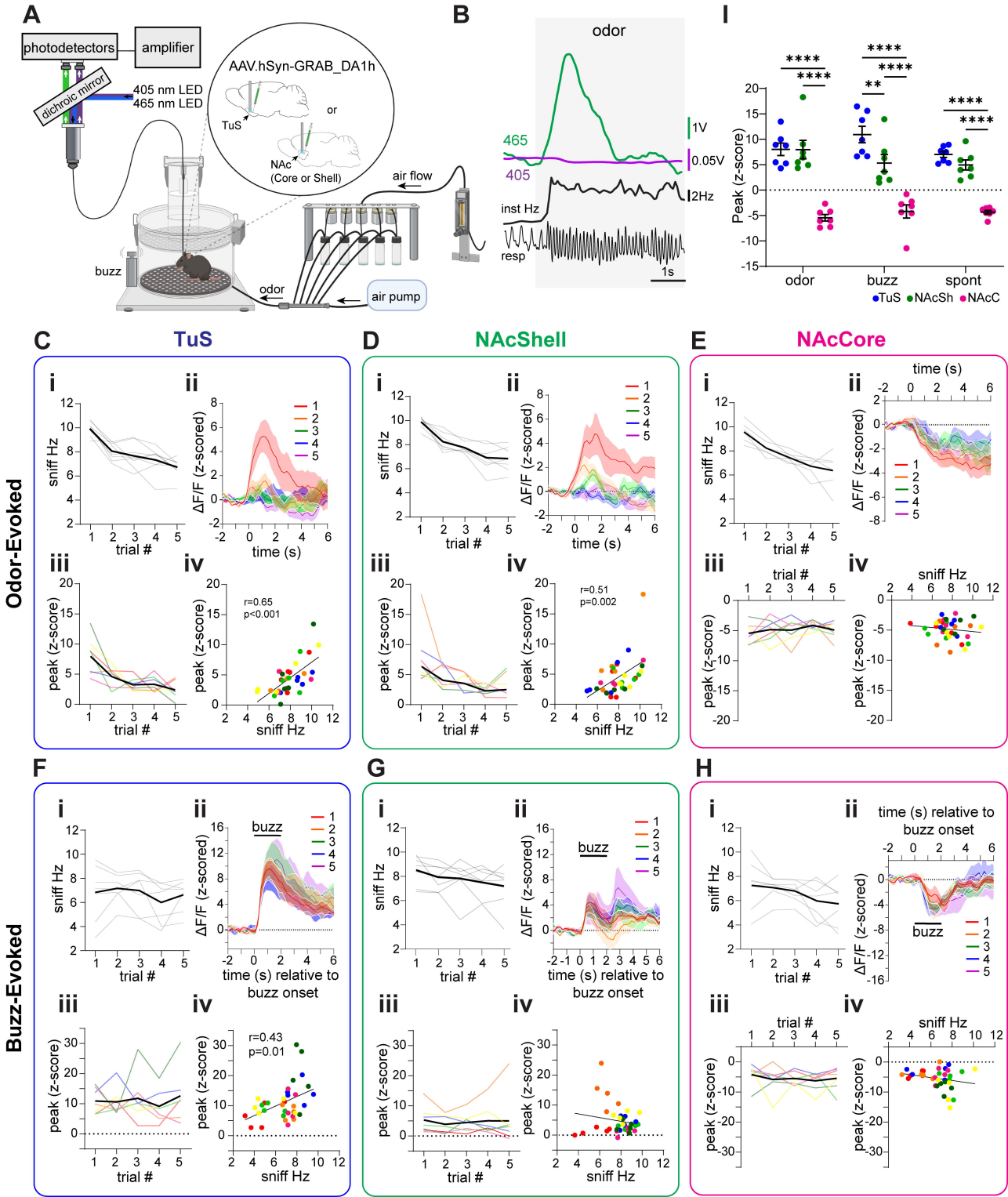

Johnson et al., Figure 4

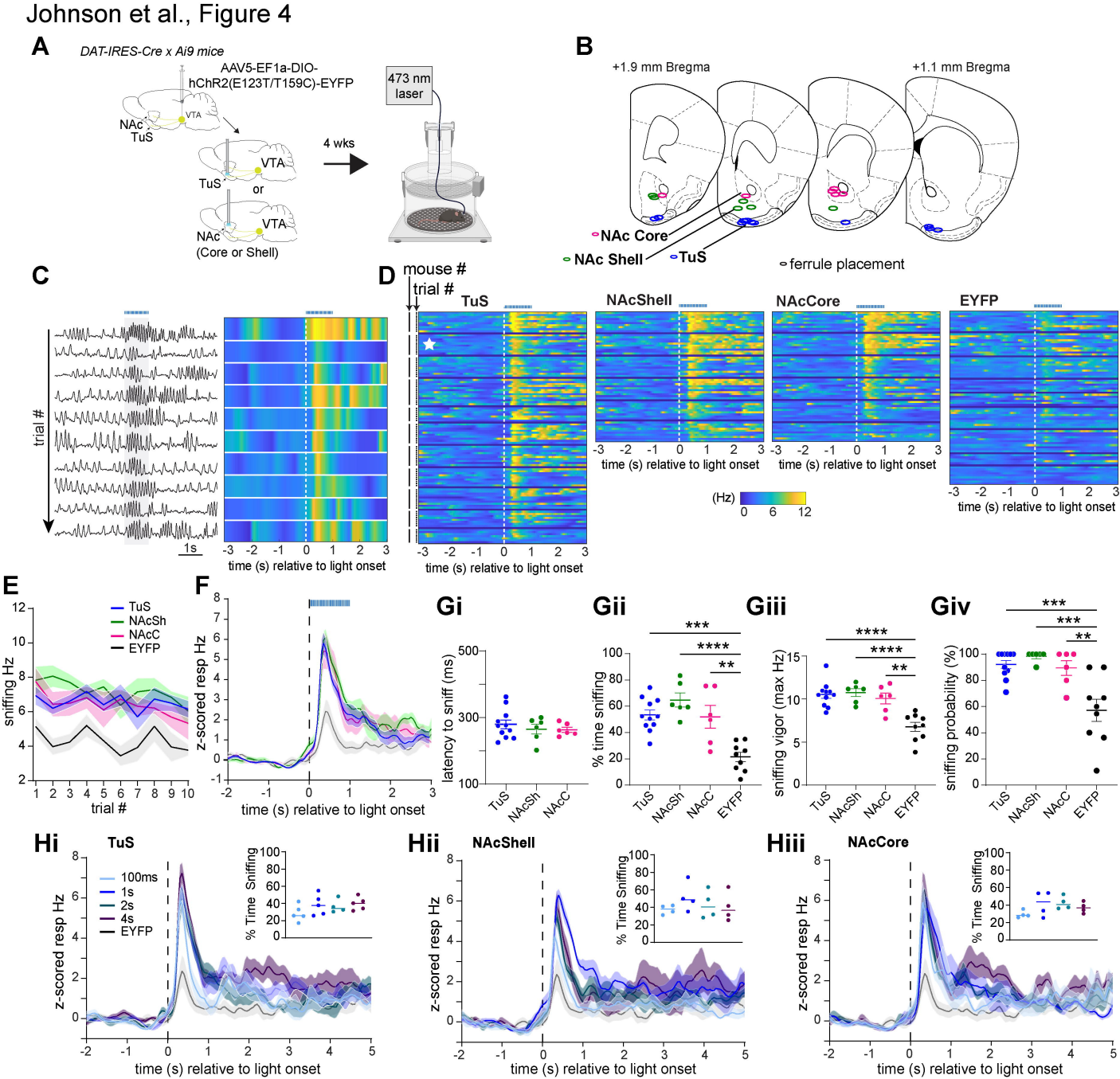

Johnson et al., Figure 5

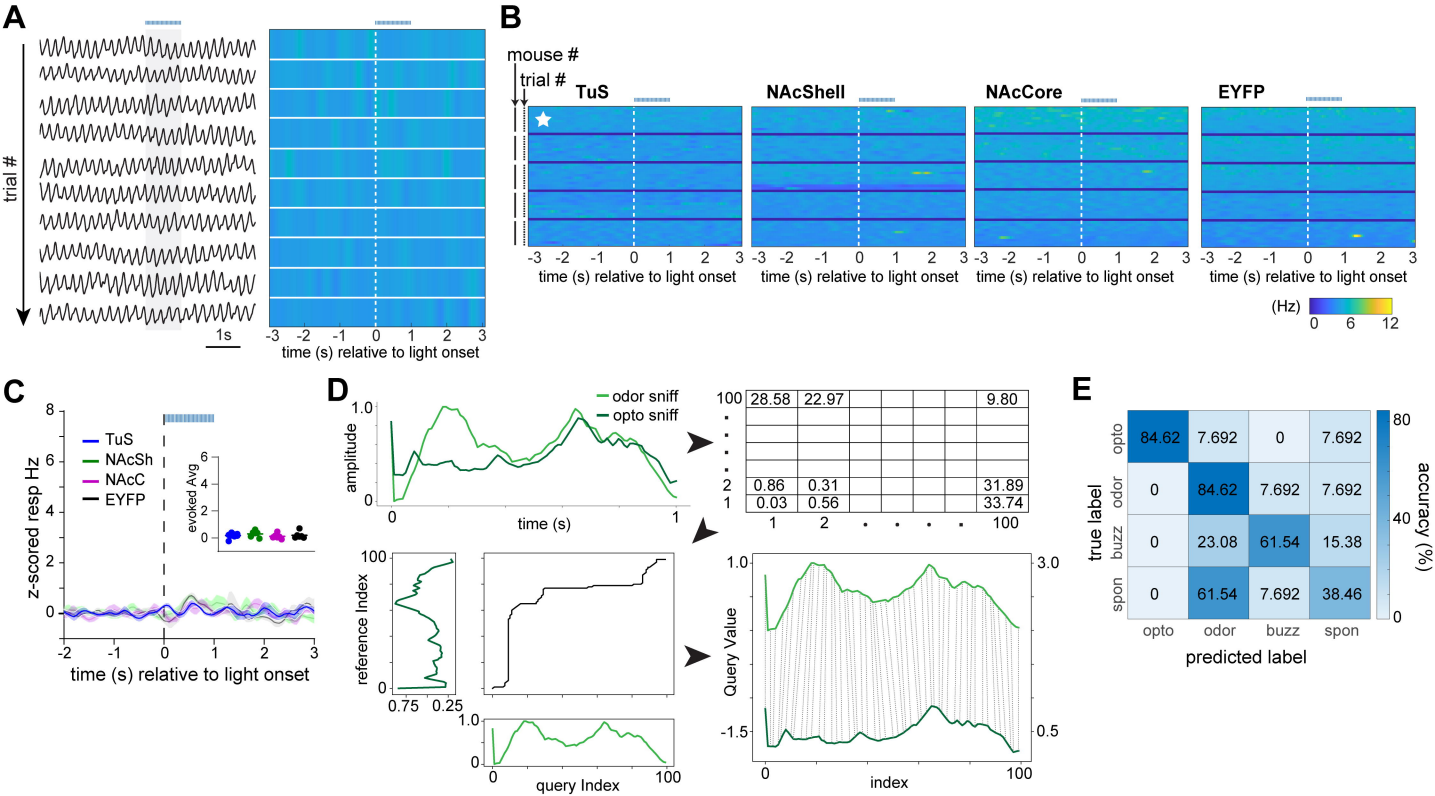

Johnson et al., Figure 6

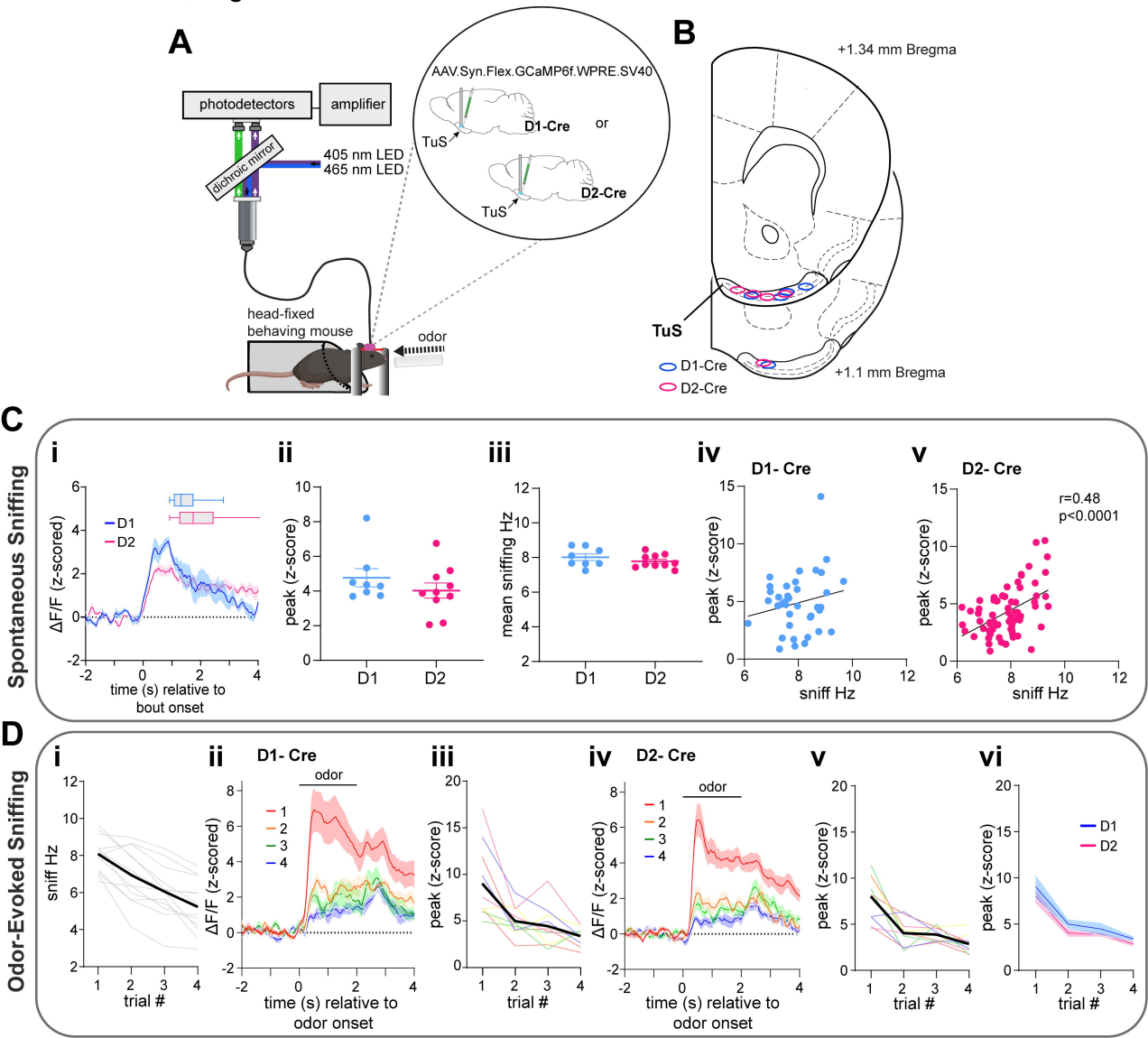
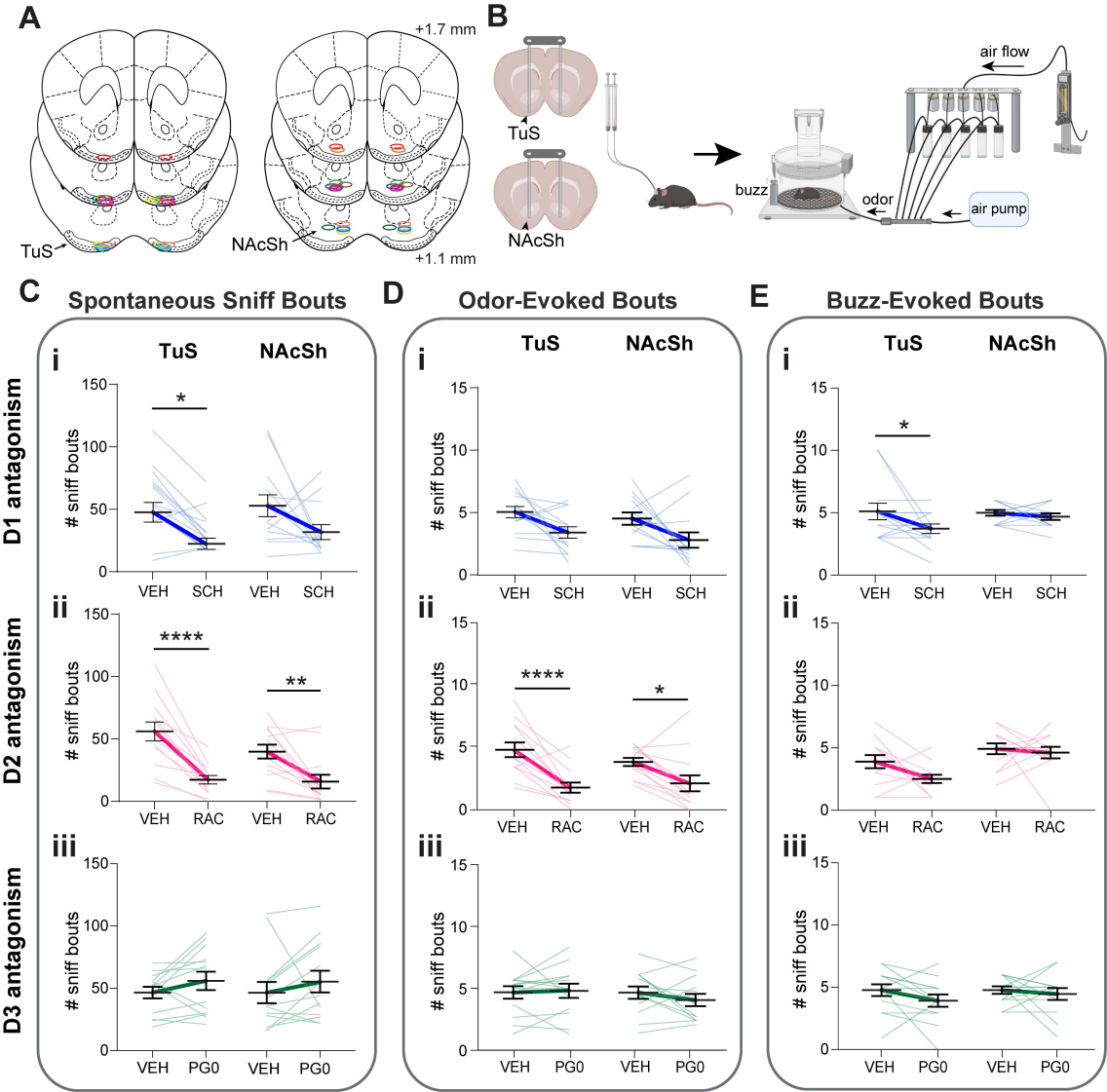
Johnson et al., Figure 7